

2018

Intracellular localization and effects of the trace-amine associated receptor 1

<https://hdl.handle.net/2144/31290>

"Downloaded from OpenBU. Boston University's institutional repository."

BOSTON UNIVERSITY
SCHOOL OF MEDICINE

Thesis

**INTRACELLULAR LOCALIZATION AND EFFECTS OF THE TRACE-
AMINE ASSOCIATED RECEPTOR 1**

by

SHANE SHAKAR SCOTT

B.S., Brandeis University, 2013

Submitted in partial fulfillment of the
requirements for the degree of
Master of Science

2018

© 2018 by
SHANE SHAKAR SCOTT
All rights reserved

Approved by

First Reader

Vickery Trinkaus–Randall, Ph.D.
Professor of Biochemistry

Second Reader

Susan G. Amara, Ph.D.
Scientific Director
National Institutes of Mental Health, NIMH

Third Reader

Suzanne M. Underhill, Ph.D.
Senior Research Fellow
National Institutes of Mental Health, NIMH

DEDICATION

I would like to dedicate this work to my mentor and inspiration Dr. Ben Barres. For it is your grace and spirit that actualized a place in science for me. Thank you for showing me that science can and should embody ALL people.

ACKNOWLEDGMENTS

On journeys worth voyaging, it is only fitting that we embark on them with those who have seen rough waters and returned. The journey to complete this thesis would not have been possible without experienced voyagers like Dr. Susan G. Amara, Dr. Suzanne M. Underhill, and Dr. Janet Clark. These women, in their own ways, have paved the path for the successful completion of this work. Dr. Underhill and Dr. Amara, provided me with preliminary data for thesis development and guided me continuously towards compiling the data on the work herein. Meanwhile Dr. Clark's unwavering support allowed me to return to the NIH to complete this work.

I want to express my special thanks to Dr. Underhill for all her patience, time, motivation and immense knowledge. Her guidance was instrumental at both the research and writing stages of my thesis. I cannot imagine having had a better advisor and mentor. Thank you for challenging me each day. It goes without saying that I express my full-hearted gratitude to Dr. Amara for her constant encouragement and direction as I did this work in her laboratory.

In addition, I would like to thank Dr. Vickery Trinkaus-Randall, Dr. Gwynneth Offner and Dr. Karen Symes for their insightful comments and encouragement throughout the completion of my master's degree and thesis.

I would also like to thank my fellow lab colleagues Dr. Jingshan Chen and Carla Glasser for providing me with important resources as well as, invaluable help and support as I completed this thesis work. To all my other lab mates, thank you for stimulating

discussions and for supporting me in my life in general. I am particularly grateful to Dr. Jennie Garcia Olivares for listening to my ramblings and providing me with career and life advice.

Lastly, I would like to thank God and my created family: my parents, my grandmother, my siblings, Tawanna Johnson, Dr. Sharon Milgram, Dr. Michael Sheridan, and Lamia Harper for all their prayers, encouragement and spiritual support. To my dear friends, Jobert Vargas, Carter Clinton, and Brooklyn Tyler thank you for constantly reminding me of the purpose in my journey.

Thank you all!

**INTRACELLULAR LOCALIZATION AND EFFECTS OF THE TRACE-AMINE
ASSOCIATED RECEPTOR 1**

SHANE SHAKAR SCOTT

ABSTRACT

The trace amine-associated receptor 1 (TAAR1) is an intracellular G-protein coupled receptor whose activation by trace amines, catecholamines and amphetamines leads to elevation of cyclic-AMP and activation of protein kinase A (PKA). Recently, the Amara lab discovered that TAAR1 also mediates the activation of the small GTPase, RhoA. TAAR1 is expressed in midbrain dopamine (DA) neurons, including those in the substantia nigra and ventral tegmental area, and thus is positioned to modulate both motor activity and addiction-related plasticity. Due to antibody limitations, however, neither the intracellular membrane localization of TAAR1 nor the site of signaling by this receptor has been clearly demonstrated in neurons.

Dopaminergic neurotransmission is a coordinated process which requires synthesis, packaging, exocytosis, and reuptake of DA. Amphetamine (AMPH) can stimulate TAAR1, which has been shown to downregulate the surface expression of the dopamine transporter, thus decreasing DA reuptake and increasing extracellular DA concentrations. In addition, AMPH and elevation of cAMP decreases the activity of the vesicular monoamine transporter, VMAT₂ in neurosecretory pheochromocytoma (PC12) cells, although the mechanism of this regulation remains undefined. The co-expression of TAAR1 and VMAT₂ in the DA neuron and PC12 cells suggests that TAAR1 activation

may mediate the effects of AMPH/cAMP on VMAT₂. Towards understanding the role of TAAR1 in transporter trafficking and function in the DA neuron, this thesis seeks to define the mechanism of AMPH action on TAAR1 signaling and examine the intracellular membrane localization and pathways downstream of TAAR1 activation.

In Chapter I, we used compartment-specific FRET-based sensors to determine the functional subcellular localization of TAAR1. Novel endomembrane targeting constructs were designed and targeting, and functionality was confirmed using standard biochemical techniques and confocal microscopy. Targeted FRET-based sensors for PKA and RhoA activation enabled us to assess TAAR1-mediated responses to AMPH treatment in discrete subcellular compartments. AMPH increased PKA activation in the synaptic vesicle compartment. However, TAAR1-mediated effects of AMPH on RhoA signaling was differentially localized to the Golgi and ER membrane compartments.

In Chapter II, it was hypothesized that PKA activation of TAAR1 may negatively regulate VMAT₂. We used midbrain DA neuron cultures and SK-N-SH neuroblastoma cells that express TAAR1 and VMAT₂ and release catecholamines as model systems. With CRISPR-Cas9 technology the Amara lab generated TAAR1 knockout SK-N-SH cells that were used to examine the role of TAAR1 in VMAT₂ regulation. VMAT₂-mediated uptake of radiolabeled DA and serotonin was measured in the presence or absence of drugs that modulate VMAT₂ activity. Inhibition of the G α stimulatory (G α _s) G-proteins upstream of PKA activation increased VMAT₂ uptake; conversely, stimulation of cAMP decreased VMAT₂ activity. Compared to wildtype cells, we found no difference in VMAT₂ uptake in TAAR1 knockout cells treated with PKA agonists like

dibutryl cAMP and forskolin. These data suggest that VMAT₂ uptake is modulated by G_αs signaling, cAMP and PKA activation, but does not require TAAR1. Taken together our results show that the cAMP-dependent inhibition of VMAT₂ uptake by PKA is not mediated by the TAAR1 receptor.

TABLE OF CONTENTS

TITLE.....	i
COPYRIGHT PAGE.....	ii
READER APPROVAL PAGE.....	iii
DEDICATION.....	iv
ACKNOWLEDGMENTS.....	v
ABSTRACT.....	vii
TABLE OF CONTENTS.....	x
LIST OF TABLES.....	xii
LIST OF FIGURES.....	xiii
LIST OF ABBREVIATIONS.....	xv
CHAPTER ONE: INTRODUCTION.....	1
TAAR1 expression.....	1
TAAR1 activation and behavior.....	2
TAAR1 in transporter and receptor membrane localization.....	3
TAAR1 agonist-induced PKA and RhoA signaling.....	4
Components of PKA and RhoA signaling are localized to discrete compartments ...	5
Förster (or Fluorescence) Resonance Energy Transfer (FRET).....	6
CHAPTER ONE: SPECIFIC AIMS.....	7

MATERIALS & METHODS	8
RESULTS	17
DISCUSSION.....	23
CHAPTER TWO: INTRODUCTION.....	48
VMAT Function and Location.....	48
VMAT Regulation	49
VMAT ₂ and TAAR1	50
CHAPTER TWO: SPECIFIC AIMS	52
MATERIALS & METHODS	53
RESULTS	57
DISCUSSION.....	62
APPENDIX.....	72
LIST OF JOURNAL ABBREVIATIONS.....	74
REFERENCES	77
CURRICULUM VITAE.....	86

LIST OF TABLES

Table	Title	Page
1	Targeting motifs	32

LIST OF FIGURES

Figure	Title	Page
1.1	TAAR1 structure and ligands	29
1.2	Subcellular targeting of PKA signaling through AKAPs	30
1.3	A-Kinase Activity Reporter 4 (AKAR4) FRET biosensor	31
1.4	Mitochondrial targeting of AKAR4	33
1.5	Localization of Golgi-AKAR4	34
1.6	Characterization of the Nuclear-AKAR4 biosensor	35
1.7	Cellular distribution of SV-AKAR4	36
1.8	Organelle-specific intramolecular PKA biosensors are stimulated by cAMP	37
1.9	AMPH-mediated PKA activation requires DAT	38
1.10	PKA-FRET biosensors do not show preferential responses to AMPH in HEK293 cells	39
1.11	PKA activation in response to AMPH favors synaptic vesicles in SK-N-SH cells	40
1.12	RhoA-2 FRET biosensor	41
1.13	Localization of the MitoRhoA-2 reporter	42
1.14	GolgiRhoA-2 localizes to the Golgi apparatus	43
1.15	NuclearRhoA-2 and SVRhoA-2 cellular distribution	44

1.16	RhoA biosensor response to AMPH is most robust in the ER/Golgi membranes in HEK293 cells	45
1.17	AMPH-induced RhoA biosensor activity favors the ER/Golgi domains in SK-N-SH cells	46
1.18	RhoA activation in response to AMPH is attenuated in TAAR1 KO SK-N-SH cells	47
2.1	cAMP-dependent downregulation of VMAT ₂ activity in MB DA neurons	67
2.2	G _{αs} G-proteins downregulate reserpine-sensitive VMAT ₂ uptake	68
2.3	Time course of reserpine inhibition of VMAT ₂ DA uptake in SK-N-SH cells	69
2.4	Deletion of TAAR1 does not change the morphology or expression of VMAT ₂	70
2.5	TAAR1 does not mediate cAMP-dependent VMAT ₂ uptake in SK-N-SH cells	71

LIST OF ABBREVIATIONS

5-HT	5-Hydroxytryptamine (aka Serotonin)
AADC	Aromatic Amino Acid Decarboxylase
AC	Adenylate Cyclase
AKAPs	A-Kinase Anchoring Proteins
AKAR4	A-Kinase Activity Reporter 4
AMPA	α -Amino 3-hydroxy-5-Methyl-4-isoxazolepropionic Acid
AMPH	Amphetamine
ATP	Adenosine Triphosphate
AUC	Area Under the Curve
cAMP	Cyclic Adenosine Monophosphate
Cas9	CRISPR associated protein 9
cDNA	Complementary Deoxyribonucleic Acid
CFP	Cyan Florescent Protein
cMYC	cMYC proto-oncogene
CNS	Central Nervous System
CRISPR	Clustered Regularly Interspaced Short Palindromic Repeats
DA	Dopamine
D-AKAP1	Dual A-Kinase Anchoring Protein 1
DAPI	4',6-Diamidino-2-Phenylindole
DAT	Dopamine Transporter
dbCAMP	Dibutyl Cyclic Adenosine Monophosphate

DMEM	Dulbecco's Modified Eagle's Medium
DOPA.....	Dihydroxyphenylalanine
DRD1	Dopamine Receptor D1
EAAT3.....	Excitatory Amino Acid Transporter 3
eCFP.....	Enhanced Cyan Florescent Protein
EDTA	Ethylenediaminetetraacetic Acid
eNOS.....	Endothelial Nitric Oxide Synthase
ER	Endoplasmic Reticulum
FBS	Fetal Bovine Serum
FCCP.....	Carbonyl cyanide-4-(trifluoromethoxy)phenylhydrazone
FHA1.....	Forkhead Associated phosphopeptide binding domain 1
FRET.....	Förster (or Fluorescence) Resonance Energy Transfer
GAPDH.....	Glyceraldehyde 3-phosphate Dehydrogenase
GDP.....	Guanosine Diphosphate
GEF.....	Guanine Nucleotide Exchange Factor
GFP	Green Fluorescent Protein
GPCR	G-protein Coupled Receptor
GTP.....	Guanosine Triphosphate
HEK293	Human Embryonic Kidney 293
HRP.....	Horseradish Peroxidase
KCL.....	Potassium Chloride
KO.....	Knockout

KRAS.....	Kirsten Rat sarcoma viral oncogene homolog
LCDV.....	Large Dense Core Vesicles
LYN.....	Lck/Yes Novel Tyrosine Kinase
MAO.....	Monoamine Oxidase
MB.....	Midbrain
METH.....	Methamphetamine
MPP.....	1-Methyl-4-Phenylpyridinium
MPTP.....	1-Methyl-4-Phenyl-,2,3,6-Tetrahydropyridine
mRNA.....	Messenger Ribonucleic Acid
NAc.....	Nucleus Accumbens
NE.....	Norepinephrine
NGS.....	Normal Goat Serum
NIH.....	National Institutes of Health
NLS.....	Nuclear Localization Sequence
NMDA.....	N-Methyl-D-Aspartate
NT.....	Neurotransmitter
OMM.....	Outer Mitochondrial Membrane
PAABD.....	Phosphopeptide-Binding Domain
PBS.....	Phosphate-Buffered Saline
PBSK.....	Phosphate-Buffered Saline with KCL
PC12.....	Pheochromocytoma 12
PDE.....	Phosphodiesterase

PFA	Paraformaldehyde
PFC	Prefrontal Cortex
PKA	Protein Kinase A
PM	Plasma Membrane
pmAC	Plasma–membrane Adenylate Cyclase
PNS	Peripheral Nervous System
qPCR	Quantitative Polymerase Chain Reaction
RBD	Rho–Binding Domain
RH	Regulator of G–protein Signaling Homolog Domain
RhoA	Ras Homolog gene family, member A
RpCAMP	cAMPs–Rp, Triethylammonium Salt
RT	Room Temperature
sAC	Soluble Adenylyl Cyclase
SEM	Standard Error of Measurement
SK–N–SH	Human Neuroblastoma Cell Line
SN	Substantia Nigra
SSV	Small Synaptic Vesicle
SV	Synaptic Vesicle
TA	Trace Amines
TAAR1	Trace Amine–Associated Receptor 1
TAT	Transactivator of Transcription
TH	Tyrosine Hydroxylase

TM.....	Transmembrane
Tom20.....	Translocase of Outer Membrane 20
VMAT ₁	Vesicular Monoamine Transporter 1
VMAT ₂	Vesicular Monoamine Transporter 2
VTA.....	Ventral Tegmental Area
YFP.....	Yellow Florescent Protein
β-PEA.....	β-Phenylethylamine

CHAPTER ONE: INTRODUCTION

Historical Background

The simultaneous discovery of the novel trace amine-associated receptor 1 (TAAR1) by two independent groups in 2001 opened doors to deciphering the roles of endogenous trace amines (TAs) in the monoaminergic systems (Figure 1.1A) [1,2]. TAAR1, a phylogenetically conserved G-protein coupled receptor (GPCR), is activated by TAs like ρ -tyramine, β -phenylethylamine (β -PEA), octopamine and tryptamine [3]. TAs are present in trace amounts in the mammalian brain and share structural and metabolic similarities with classic monoamines including DA, which is also a TAAR1 agonist [1–3]. Like DA, TA's are also degraded by monoamine oxidase (MAO) enzymes (Figure 1.1B) [4,5]. Prior to TAAR1's discovery, initial studies linked TAs to increased sympathomimetic actions in the peripheral nervous system (PNS) where TAs modulated the release of norepinephrine (NE) in peripheral synapses [6,7]. The consequence of excessive ρ -tyramine extracellular release of NE results in a hypertensive crisis called the “*tyramine storm*,” experienced by patients who consume copious amounts of aged cheese containing ρ -tyramine while adhering to treatments with monoamine oxidase inhibitors that would normally degrade tyramine (Figure 1.1B) [6–8].

TAAR1 expression

TAAR1 mRNA and protein is expressed in the central nervous system (CNS), albeit in low levels compared to the PNS [1,2,9–11]. Using quantitative polymerase chain reaction (qPCR) analysis and mRNA *in situ* hybridization studies, Bunzow and

colleagues showed that TAAR1 mRNA was expressed in the monoaminergic nuclei of locus coeruleus, nucleus accumbens (NAc), prefrontal cortex (PFC), ventral tegmental area (VTA), and substantia nigra (SN) [2]. Later, using a LacZ–driven reporter for TAAR1 it was demonstrated that TAAR1 protein is also present in hypothalamus, amygdala, preoptic area and dorsal raphe nucleus [9]. Surprisingly, TAAR1 was also shown to be predominately localized intracellularly, and it appeared to be coupled to G α stimulatory (G α _s) heterotrimeric G–proteins [1,2,11]. This knowledge prompted the search for TAAR1’s intracellular membrane localization. Work by Szumska and colleagues described that in thyrocytes, TAAR1 is present in membranes of subcellular compartments that function in the secretory pathway as well as, in the apical plasma membrane [12]. Using TAAR1 specific antibodies, it was shown that TAAR1 localized to the endoplasmic reticulum (ER), the Golgi apparatus, and transport vesicle–like structures that lined up along the borders of neighboring thyrocytes but was absent from endosomal vesicles [12]. However, the subcellular and functional localization of TAAR1 in neurons remains unknown due to both the limitations of the antibodies as well as, low levels of TAAR1 protein expression in brain [1,2].

TAAR1 activation and behavior

Along with TAs, the biogenic amines and psychostimulants, including dopamine (DA), methamphetamine (METH), and amphetamine (AMPH), also activate TAAR1 [1,2,10,13]. In a subset of DA neurons in murine and primate brain TAAR1 is expressed with DAT [13]. Accordingly, animal behavior studies implicate TAAR1 as a neuromodulator of DA neurotransmission in the mesolimbic pathway, where activation

of TAAR1 inhibits DA neuron firing [9,14]. TAAR1 contributes to the pathophysiology and addictive properties of amphetamine type drugs and modulates the degeneration of DA neurons [15]. TAAR1 knockout mice are hypersensitive to AMPH, as measured by intracerebral microdialysis, where administration of AMPH increased extracellular DA and norepinephrine levels compared to wildtype mice [9,16]. Activation of TAAR1 by METH results in inhibition of DA uptake and DA efflux through the DAT transporter [10,13]. Furthermore, inhibition of TAAR1 by antagonists, increases the rate of cocaine and METH self-administration and promotes relapse of this addictive behavior [17,18]. In this regard, TAAR1 represents a potential therapeutic target for treatment of AMPH and METH drug addiction.

TAAR1 in transporter and receptor membrane localization

Xie and Miller first demonstrated the role of TAAR1 in regulation of dopamine transporter (DAT) trafficking and surface expression in 2009 [13]. TAAR1 knockout mice treated with AMPH lost the ability to internalize DAT [13]. Wheeler and Underhill later showed that DAT internalization required AMPH-mediated activation of a small GTPase, RhoA and its reciprocal inactivation by PKA [19]. Recently, the Amara lab demonstrated that TAAR1 activation by AMPH is responsible for increased RhoA signaling and DAT internalization (unpublished). In human embryonic kidney 293 (HEK293) and SK-N-SH neuroblastoma cells transiently transfected with DAT, AMPH-induced DAT internalization is abolished in the absence of TAAR1 (unpublished). Glutamate receptors and transporters in neurons of the striatum are also regulated by

TAAR1, suggesting that DA is not the only neurotransmitter system affected in AMPH drug sensitization and addiction [15,20]. For example, Underhill and colleagues showed that AMPH induces internalization of the excitatory amino acid transporter 3 (EAAT3) [21], which increases glutamate N-methyl-D-aspartate (NMDA) receptor mediated synaptic currents in the VTA and substantia nigra pars compacta [22]. Additionally, changes in NMDA and α -amino-3-hydroxy-5-methyl-4-isoxazolepropionic acid (AMPA) receptor compositions have been reported in the striatum of TAAR1 KO mice treated with AMPH [15,20].

TAAR1 agonist-induced PKA and RhoA signaling

TAAR1 couples to G_{α_s} [1,2] and $G_{\alpha_{13}}$ (unpublished) heterotrimeric G-proteins. Activation of TAAR1 leads to activation of the G_{α_s} G-protein and stimulates adenylyl cyclase (AC), which catalyzes the formation of cyclic-AMP from adenosine triphosphate (ATP). The increase in cAMP activates protein kinase A (PKA) signaling [1,2]. Use of PKA-based FRET sensors by the Amara lab showed that TAAR1 is the intracellular target of AMPH responsible for the increases in PKA activation (unpublished). Notably, TAAR1 is also coupled to $G_{\alpha_{13}}$ G-proteins that are responsible for activation of RhoA (unpublished). TAAR1-mediated activation of RhoA in response to AMPH is also responsible for DAT and EAAT3 internalization (unpublished). Current data suggest that DAT dependent entry of AMPH into the cell leads to the activation of $G_{\alpha_{13}}$ coupled TAAR1 receptors (unpublished) and elevates RhoA signaling as well as G_{α_s} -PKA activation [19]. TAAR1-mediated activation of PKA in response to AMPH inactivates RhoA signaling [19]. Therefore, AMPH action on internalization requires a balance of

RhoA activation and PKA-dependent RhoA inactivation that are both mediated by TAAR1 [19].

Components of PKA and RhoA signaling are localized to discrete compartments

The ability of TAAR1 to activate both RhoA and PKA signaling is presumed to be dependent on the ability of GPCRs to adopt various conformational states [23,24]. TAAR1 is associated with an intracellular membrane and largely absent from the plasma membrane of transfected cells [25], indicating that the signaling components of TAAR1 maybe localized to a specific membrane compartment of the cell. The predominant models of $G\alpha_s$ -AC-cAMP require diffusion of cAMP from the plasma-membrane activated AC (pmAC). However, soluble AC (sAC) provides another means of signaling that is not at the plasma membrane and might be more amenable to the intracellular localization of a $G\alpha_s$ -coupled GPCR. G-proteins localized to organelle membranes [26,27] and signaling through sACs provides a basis for both specific, selective and discrete generation of cAMP in the cell [28-31]. A Kinase Anchoring Proteins (AKAPs) that localize PKA to the endomembrane of organelles (Figure 1.2) also provide for activation of PKA in discrete compartments [32,33]. We hypothesized that subcellular targeting of cAMP or PKA reporters may provide information about compartment specific activation of TAAR1 $G\alpha_s$ -AC-cAMP/PKA signaling in response to AMPH.

RhoA is activated by family of guanine nucleotide exchange factors (GEFs) known as regulator of G-protein signaling (RGS)-homology domain (RH) containing guanine nucleotide exchange factors (RH-RhoGEFs) [34-36]. Current research suggests that RH-RhoGEFs are ubiquitous in the cytosol and provide a direct functional link

between $G\alpha_{13}$ coupled GPCRs receptors and intracellular RhoA activation and signaling [34]. Following activation of $G\alpha_{13}$ coupled receptors or expression of constitutively active $G\alpha_{13}$ G-proteins, RH-RhoGEFs translocate to the endomembrane surface where they interact with GTP-bound $G\alpha_{13}$ G-proteins [34–39]. In this regard, it possible that activation of intracellular membrane bound $G\alpha_{13}$ coupled TAAR1 receptors may facilitate localized activation of RhoA.

Förster (or Fluorescence) Resonance Energy Transfer (FRET)

Förster (or Fluorescence) resonance energy transfer (FRET) is a process in which non-radiative energy is transferred between donor and acceptor fluorophores, for example CFP and YFP (Figure 1.3A). FRET biosensors have contributed to our understanding of spatial and temporal dynamics of signaling molecules in live cells [40–44]. An intramolecular A-kinase Activity Reporter 4 (AKAR4) FRET biosensor was developed to examine real-time of PKA activity in single cells [41,42]. It has been further modified with the addition of targeting motifs to examine compartmentalization of PKA activation [42]. RhoA-based FRET biosensors have also been developed [43,45]. The general structure of both of these biosensors sandwiches a recognition sequence for PKA phosphorylation or activated RhoA between two fluorescent proteins with proper spectral overlap between donor emission and acceptor excitation [40,41,43]. In this study, we developed new targeted FRET sensors to monitor TAAR1-mediated compartmentalized PKA and RhoA activity in response to AMPH.

CHAPTER ONE: SPECIFIC AIMS

TAAR1 has been implicated in the pathophysiology of AMPH-related addiction and is necessary for maintenance of DA neuronal plasticity. As previously described, AMPH activation of TAAR1 regulates the trafficking of transporters whose functions are integral for proper dopaminergic neurotransmission in the mammalian brain. To better understand the role of TAAR1 in dopaminergic neurotransmission, we sought to examine the intracellular localization and functional compartmentalization of TAAR1 activation *in vitro*. Through the specific aims listed below for chapter one, we seek to address this gap.

The specific aims of chapter one are to:

- 1) Identify organelle-targeting motif sequences.
- 2) Design and characterize specific organelle-targeted PKA and RhoA FRET sensors.
- 3) Test the ability of PKA and RhoA FRET sensors to respond to AMPH.
- 4) Use a CRISPR-Cas9 knockout TAAR1 cell line to assess the role of TAAR1 in AMPH stimulated RhoA and PKA activation.

A growing body of literature indicates that TAAR1 plays a role in several neuro-addictive pathologies and is a promising candidate to target for treatment of these disorders [3,7]. The outcome of this study will allow us to further delineate the mechanism of action of AMPH on TAAR1 signaling and adds to our understanding of TAAR1 cell biology. Therefore, knowledge of intracellular membrane localization may assist us in evaluating and developing tools for pharmacotherapies targeting the TAAR1 receptor.

MATERIALS & METHODS

Materials

Antibodies: Mouse monoclonal anti- α -Tubulin antibody was purchased from Sigma Aldrich (cat# T6074). Mouse anti-Golgin-97 primary antibody (cat# A-21270) was purchased from Invitrogen/ThermoFischer Scientific. Rabbit polyclonal anti-Green Fluorescent Protein (Anti-GFP) antibody was purchased from Marine Biological Laboratory (cat# 598). Mouse monoclonal GM130 (cat# ab31561), and rabbit anti-VMAT₂ (cat# ab191121) antibodies were purchased from Abcam. Rabbit anti-GAPDH (cat# G9545) and rabbit β -actin (cat# 4967L) antibodies were acquired from Sigma Aldrich and Cell Signaling respectively. The secondary antibodies donkey anti-mouse (cat# 715-035-150) horseradish peroxidase (HRP) and donkey anti-rabbit HRP (cat# 31458) were acquired from Jackson Immuno Research Laboratories Inc and Pierce, respectively.

Other reagents: dbcAMP, a cell permeable cyclic AMP analogue (cat# D026) was acquired from Sigma Aldrich. Reagents for SDS-PAGE, Bicinchoninic Bradford Protein Assay, LipofectamineTM 2000, Dulbecco's Modified Eagle's Medium (DMEM), MitoTrackerRed CMXRos (cat# M7512), Fetal Bovine Serum (FBS) and all other culture media were purchased from Invitrogen/Life Technologies. cCompleteTM, Mini, EDTA-free Protease Inhibitor Cocktail (cat# 11836170001) was acquired from Roche Diagnostics. RhoA activator I (cat# CN01) and mitochondrial isolation kit (cat# 89874) were acquired from Cytoskeleton Inc and Pierce/Thermofischer Scientific, respectively.

All other reagents were purchased from Sigma Chemical Co. (St. Louis, MO) unless otherwise stated.

Methods

Targeted FRET sensors: pcDNA3.1(+)-AKAR4 was a gift from Jin Zhang (Addgene# 61619) [41]. We designed two nuclear targeted AKAR4 reporters using the C-terminal nuclear localization sequence (NLS) of human cMYC proto-oncogene that codes for the amino acids PAAKRVKLDP or a C-terminal sequence of the SV40 Large T-antigen that codes for the amino acids PKKKRKVEDP. These targeting sequences were fused to the C-terminus of the AKAR4 plasmid followed by a stop codon before the EcoRV restriction site (Table I; Figure 1.3A). We observed that cMYC-AKAR4 exhibited less cytosolic fluorescence in comparison to SV40 AKAR4. Previous reports were that the cMYC-eGFP chimeras exhibited an increase in nuclear intensity by 160 % compared to that of the cytosol when compared to the eGFP-SV40 antigen NLS chimeras [46]. Therefore, all FRET experiments presented in this study were done with the cMYC-AKAR4 (Nuclear-AKAR4) construct. Worthy of note, we did not target the AKAR4 sensor to the outer membrane of the nucleus since it is contiguous with the ER membrane.

Two Golgi targeting AKAR4 plasmids were designed using either the first 32 amino acids from endothelial nitric oxide synthase (eNOSAKAR4) [47,48] or the C-terminal amino acids of Golgi resident protein Giantin (GiantinAKAR4). The eNOS and Giantin targeting motifs were subcloned to the N- and C-terminus of the AKAR4

plasmid, respectively. The eNOSAKAR4 showed an increased amount of cytosolic expression compared to GiantinAKAR4 and did not colocalize with *trans*-Golgi marker Golgin-97 (See Appendix 1A). Therefore, in all experiments conducted in this study the GiantinAKAR4 construct was used and named Golgi-AKAR4. We also generated two mitochondrial PKA sensors using a motif derived from N-terminal amino acids (1-30) of the mitochondrial A-kinase anchoring protein 1 (D-AKAP1) or the first thirty-three amino acids of Tom20, an outer-membrane mitochondrial (OMM) protein. Both sensors directed the AKAR4 reporter to cytosolic face of mitochondria [41,49-51]. For the experiments described in this study, the Tom20 targeted AKAR4 was used (Mito-AKAR4). The mitochondrial targeting motifs were fused to the N-terminus of the AKAR4 sensor between the *HindIII* and *BamHI* sites (Figure 1.3A).

The synaptic vesicle (SV) targeted AKAR4 reporter was generated by subcloning a forty-four amino acid localization motif from the vesicular monoamine transporter 2 (VMAT₂) to the C-terminus of the AKAR4 plasmid. All reporters generated were sequenced verified using the following primers: Forward 5'-CCACTTTGAATTTCTCTCCAC-3' and Reverse 5'-ATTTGTGATGCTATTGCTTTATTTGTAACC-3' (Macrogen USA, Rockville, MD). The lipid-raft membrane reporter(Lyn-AKAR4) and the non-lipid raft membrane reporter (Kras-AKAR4) plasmids were gifts from Jin Zhang (Addgene# 61620 and #61621, respectively) [42].

An enhanced RhoA FRET sensor (RhoA-2) was a gift from Dr. Mark Rizzo. The Rizzo lab replaced the enhanced cyan florescent protein (eCFP) with the brighter third

generation fluorophore mCerulean3 [52]. A schematic of the plasmid map is shown in Figure 1.12A. To target the RhoA-2 biosensors to the mitochondria, the N-terminal localization motif from Tom20, was used and fused to the N-terminus of the RhoA-2 plasmid between the *Pac I* and *NcoI* restriction sites (Table I; Figure 1.11A). For the GolgiRhoA-2 plasmids, the C-terminal localization motif of Giantin was used. The synaptic vesicle (SV) targeting RhoA was also generated using the cytoplasmic C-terminal localization motif of VMAT₂ and was fused to the C-terminus of the enhanced RhoA-2 FRET sensor. The ER targeting sensor was generated by Dr. Underhill in the Amara lab by fusing the N-terminal localization motif of cytochrome p450 to the RhoA-2 plasmid. All C-terminal localization motifs were subcloned into the C-terminus of the RhoA-2 plasmid following a stop codon before the *XhoI* site (Figure 1.12). All final targeted RhoA-2 plasmids were sequenced verified using the following primers: Forward 5'-GAGGTTTTTGAAATGGCTACGAG-3' and Reverse 5'-CAGGCTGCCAGCAGCTTGCAGGC-3' (Macrogen USA, Rockville, MD).

Cell Culture and Transfection: SK-N-SH and HEK293 cells were obtained from American Type Culture Collection (ATCC, Rockville, MD, U.S.A.) while TAAR1 knockout SK-N-SH cell line was generated by Dr. Jingshan Chen in the Amara lab (See details below). All cells were maintained in DMEM supplemented with 0.1 % Penicillin/Streptomycin and 5 % FBS at 37 °C in a humidified incubator containing 5 % CO₂. All cells were transfected using Lipofectamine™ 2000 according to the manufacturer's protocol, with slight modifications. In brief, plasmid DNA (1 µg) and

Lipofectamine™ 2000 (3 µL) were incubated in 50 µL of Opti-MEM (Life Technologies) separately for 5 minutes. The solutions were then combined and incubated at room temperature (RT) for 20 minutes. 20×10^6 cells were added to the solution and incubated for 1 h at room temperature (RT) before plating onto poly-D-lysine coated plates or glass coverslips. Imaging, fractionation, western blot analysis, drug treatments and immunocytochemistry were carried out between 24 to 48 h post transfection. All cell culture assays were performed on cultures from at least three different plating procedures creating at least three biological replicates. Where possible, experiments were performed under blinded conditions.

Knock Out Cell Line: Dr. Jingshan Chen in the Amara lab used CRISPR-Cas9 technology to generate the TAAR1 knockout SK-N-SH cell line. In brief, guide RNA primers that target 20–27 codons of the TAAR1 genomic DNA were designed and introduced into the SK-N-SH cells via transfection along with CRISPR associated protein 9 (Cas9) DNA endonuclease (See Appendix 2A). The Cas9-mediated double stranded breaks were repaired by non-homologous end joining and resulted in deletion of less than three nucleotides causing a frameshift that generated premature stop codons resulting in the expression of truncated, nonfunctional TAAR1 proteins (See Appendix 2A).

Immunohistochemistry: Cells were fixed in 4 % paraformaldehyde (PFA) at RT for 15 minutes. After three washes with phosphate-buffered saline (PBS), cells were permeabilized with 0.20 % Triton X-100 for 5 minutes and blocked with 5 % normal

goat serum (NGS) for 1 h at RT before incubation with primary antibodies diluted in 5 % NGS overnight at 4 °C on a shaker. Primary antibodies were washed away with PBS and secondary antibodies applied in 5 % NGS for 2 h at RT. Secondary antibodies were washed off, and the coverslips were mounted in Fluoromount™ Aqueous Mounting Medium (cat# F4680; Sigma Aldrich) for subsequent examination.

MitoTracker Labelling: Twenty–four hours post transfection, the mitochondria were identified by staining with MitoTrackerRed CMXRos, a mitochondria specific fluorescent dye. In these experiments, MitoTrackerRed CMXRos was added to the cells at a final concentration of 25 nM for 15 minutes at 37 °C. The cells were then washed five times with warm culture media and incubated under normal culture conditions for 30 minutes prior to live cell imaging. The cells were then washed with PBS and imaged as described below.

Mitochondrial Isolation: To confirm the proper localization of the mitochondrial targeting biosensors generated, we isolated mitochondrial fractions from SK–N–SH and HEK293 cells transfected with the mitochondrial targeting plasmids using a Mitochondria Isolation Kit for cultured cells according to the manufacturer’s protocol. In brief, crude mitochondrial fractions from cells transfected with mitochondrial targeted sensors were isolated in a proprietary buffer at 12, 000 × g and analyzed by immunoblotting. Purity of the mitochondrial fraction was assessed by the presence of Tom20 (a mitochondrial marker) and absence of α -tubulin (a cytosolic marker).

ER/Golgi Microsome Isolation: HEK293 cells were transfected with either GolgiRhoA-2 or Golgi-AKAR4 plasmids and plated in T75 cm² flasks. Twenty-four hours after transfection, the cells were detached with trypsin, pelleted at 600 × g for 5 minutes and washed with PBS. The pellet was subsequently used for isolation of ER/Golgi microsomal fractions using a commercially available kit (Sigma Aldrich, cat# ER0100). In brief, the cell pellet was resuspended in a hypotonic homogenization buffer containing protease inhibitor cocktail, allowed to swell for twenty minutes at 4 °C and then pelleted. The cells were resuspended in isotonic buffer containing protease inhibitor and lysed using a Dounce homogenizer. Unlysed cells and nuclear debris were separated by centrifugation at 1,000 × g for 10 minutes. The supernatant from this step was further centrifuged at 12,000 × g for 10 minutes to pellet the mitochondria. The post mitochondrial supernatant was used for precipitation of ER/Golgi microsome fraction with 8 mM calcium chloride, which was added dropwise with constant agitation at 4 °C. The ER/Golgi microsome fraction was pelleted by centrifugation at 8,000 × g for 10 minutes at 4 °C. The pellet was dissolved in a RIPA lysis buffer containing 100 mM Tris-HCL pH 7.4; 300 mM NaCl; 2 % NP-40; 1 % sodium deoxycholate and 0.2 % sodium dodecyl sulfate (RPI Research, USA). Enrichment of the ER/Golgi microsome fraction was confirmed by the presence of GM130 Golgi marker and absence of β-actin (a cytosolic marker) as well as GAPDH (a cytoplasmic marker).

Immunoblot: Immunoblotting was performed as described previously, with slight modifications [21]. Briefly, cells were homogenized in lysis buffer containing 50 mM Tris-HCl, pH 7.5, 150 mM NaCl, 5 mM EDTA, 1 % Triton X-100, 4 mM N-ethylmaleimide and protease inhibitor. Lysates were centrifuged at $20,000 \times g$ for 10 minutes at 4 °C and the supernatant fraction was used for western blots. All primary antibodies used in these experiments were used at a concentration of 1:1000 unless otherwise indicated. Following overnight incubation with primary antibodies at 4 °C, each blot was probed with the appropriate HRP-conjugated secondary antibody (1:5000) for 1 h at RT. Immunoreactive signals were visualized using Western LightningTMPlus-ECL Enhanced Chemiluminescence Substrate (Perkin Elmer, cat# NEL104001EA) and detected with a chemiluminescence imaging system (Bio-Rad Laboratories).

Live Cell Imaging and Data Analysis: Cells were washed twice with warm phenol red deficient DMEM then imaged at RT for 30–60 minutes. Cells were treated with drugs as indicated after two or five minutes of baseline FRET acquisition. Images were acquired on a Nikon AR1 equipped with a 60X/1.3 NA oil-immersion objective lens and NIS Elements Advanced Research software. Dual emission ratio imaging was performed using a 457 nm excitation filter, and two emission filters (440 nm for CFP and 617.5 nm for YFP). Images were acquired every 10 seconds. Background correction of fluorescent images was performed by subtracting the intensities of regions of the imaging field where fluorescence was absent (Formula 1).

$$FRET_{ratio} = \frac{(Accepter\ YFP - Accepter\ YFP_{BkGrd})}{(Donor\ CFP - Donor\ CFP_{BkGrd})} = \frac{YFP}{CFP} \quad \text{Formula 1}$$

The YFP/CFP ratios at each time point were normalized to the two-minute baseline levels preceding drug application (Formula 2).

$$\text{Normalized FRET} = \frac{(\text{FRET ratio}_{\text{Time (t)}})}{\text{Average } \frac{\text{YFP}}{\text{CFP}}_{\text{baseline}}} \times 100\% \quad \text{Formula 2}$$

The FRET ratios at given time (t) calculated using Formula 1 were normalized by dividing by the FRET ratios at baseline (2 minutes prior to drug treatment). Graphs of the ratio time course (ratio vs time) were plotted, and statistical analysis was performed with GraphPad Prism version 6.0 (GraphPad Software, La Jolla, CA). Selection criteria for each cell was as follows: (1) those that were saturated in either the CFP or YFP wavelength at the start of the experiment were removed from analysis; (2) cells that did not respond to subsequent treatment with dbcAMP or Rho Activator I were discounted; (3) and, for HEK293 cells, we excluded cells that responded to the classic activators but not to AMPH suggesting that these cells do not co-express the DAT transporter required for AMPH entry into the cell within the time frame of the experiment.

RESULTS

Design and localization of targeted PKA biosensors

To understand how and where TAAR1 elicits PKA activity in the cell, we targeted the A-Kinase Activity Reporter 4 (AKAR4) PKA biosensor to the Golgi, mitochondria, synaptic vesicles and nucleus using different targeting motifs (Table I). The membrane targeted motifs anchor the sensor to the cytoplasmic facing membrane of the organelle, allowing for activation by PKA [42]. The nuclear localization signal localized the nuclear reporter inside the nucleus. The Mito-AKAR4 reporter was found at the cytoplasmic face of the outer-membrane of the mitochondria of HEK293 (Figure 1.4A) and, SK-N-SH cells (Figure 1.4A) as evidenced by confocal microscopy. We further validated the specific localization of Mito-AKAR4 in HEK293 cells using a reagent-based mitochondrial isolation kit followed by immunoblotting analysis (Figure 1.4B). Probing the cytosolic and mitochondrial fractions for the green fluorescent protein (GFP) to identify the FRET sensor, Tom20 (a mitochondrial marker) and α -Tubulin (a cytosolic marker) demonstrated that Mito-AKAR4 predominantly enriched in the mitochondrial fractions. The untargeted donor AKAR4 plasmid was found in the cytosolic fraction (Figure 1.4B; Appendix 3A). Colocalization with mitochondrial marker, MitoTracker confirmed this finding (Figure 1.4C).

The Golgi-AKAR4 sensor did not appear to alter the structure of the Golgi upon overexpression (Figure 1.5A) and colocalized with the *cis*-Golgi marker GM130 (Figure 1.5A). Additionally, subcellular fractionation of the ER/Golgi membranes demonstrated that Golgi-AKAR4 was properly localized in the GM130 positive fraction of Golgi

(Figure 1.5B). The purity of the Golgi/ER microsomes was verified by the presence of GM130 and the absence of GAPDH and β -actin (Figure 1.5B).

The nuclear localization signal (NLS), PAAKRVKLD, derived from human c-Myc protooncogene protein (Table I), was fused to the C-terminus of AKAR4 to target PKA biosensors to the nucleus [46]. Nuclear AKAR4 colocalized with DAPI a DNA stain that indicates the nucleus (Figure 1.6).

Szumaska and colleagues reported that TAAR1 in thyrocytes was localized to vesicles of the secretory pathway [12]. We hypothesized that in neurons, this might be analogous to synaptic vesicles, so we also generated a AKAR4 sensor targeted to synaptic vesicles (SV-AKAR4; Table I) using a synaptic vesicle trafficking motif derived from VMAT₂ [53,54]. Proper targeting of SV-AKAR4 was verified in SK-N-SH cells, which express synaptic vesicles and endogenous VMAT₂ (Figure 1.7A). While the expression of the SV-AKAR4 biosensor was visually analogous to VMAT₂ positive synaptic vesicles (Figure 1.7A, B), at this time, confirmation of this is hampered by the lack of a viable antibody for synaptic proteins like synapsin I and synaptotagmin I.

Organelle-specific intramolecular PKA biosensors are stimulated by cAMP

Baseline FRET emissions for all PKA biosensors were stable (Figure 1.8A). The functional activity of the targeted PKA sensors was assessed in HEK293 and SK-N-SH cells by stimulation with a membrane permeable analogue of cAMP, dibutyl cAMP (dbcAMP, 1mM). HEK293 or SK-N-SH cells expressing the targeted AKAR4 sensors

were stimulated with dbcAMP and an increase in FRET emission was observed indicating functional reporters (Figure 1.8B).

PKA activation in response to AMPH is most robust near the synaptic vesicles

To activate TAAR1, AMPH must enter the neuron through the dopamine transporter (DAT) [17,49]. We co-transfected the Mito-AKAR4 biosensor with or without DAT in HEK293 cells to determine if PKA activation of the targeted AKAR4 reporter was also depended upon DAT co-expression and presumably, AMPH entry into the cell. In cells that did not express DAT, we did not observe a significant increase in Mito-AKAR4 FRET activity in response to AMPH (10 μ M) (Figures 1.9A–C), confirming previous data suggesting that DAT is required for AMPH activation of TAAR1. After twenty minutes, there is a slight increase in PKA activation in cells without DAT (Figures 1.9A and C), which was also observed in cells treated with vehicle controls (data not shown) indicating that it reflects non-specific baseline activity. The change in FRET emission normalized to a five-minute baseline was found to be 117.45 ± 1.73 % at thirty minutes for cells transfected with both DAT and Mito-AKAR4 compared to the 103.95 ± 0.85 % in cells that were not co-transfected with DAT (Figure 1.9A). Statistical analysis of the area under the curves (AUC) demonstrates significant AMPH-mediated PKA activation in the presence of DAT (Figure 1.9B; **** $p < 0.0001$). Representative images of the change in FRET YFP/CFP ratios in the presence or absence of DAT at various time points are shown in Figure 1.9C.

To ensure that all plasmids were equally co-transfected with DAT and the AKAR4 construct of interest, we assessed protein expression with western blots. No difference in co-expression was observed among the plasmids (data not shown). The organelle-targeted PKA-FRET based sensors enabled us to assess PKA responses to AMPH in different subcellular compartments including the Golgi, mitochondria, lipid-raft, non-lipid raft, nucleus and synaptic vesicle compartments (Figures 1.10 and 1.11). The most robust activation of PKA by AMPH in SK-N-SH cells occurred when the sensor was targeted to synaptic vesicles (Figure 1.11C). Maximum FRET-emission ratio for the SV-AKAR4 plasmid at thirty minutes was $158.5 \pm 8.3 \%$ (n=36), compared to $112.1 \pm 1.2 \%$ (n=18) for Golgi-AKAR4; $112.26 \pm 1.7 \%$ (n=24) for Lyn-AKAR4; $111.6 \pm 1.9 \%$ (n= 30) for Mito-AKAR4; $110.0 \pm 1.2 \%$ (n=14) for Kras-AKAR4 and $111 \pm 0.7 \%$ (n=34) for Nuclear-AKAR4. In HEK293 cells there was no significant difference in responses of the AKAR4 targeted FRET sensors; however, HEK293 cells do not possess synaptic vesicles that may preclude proper function/localization in this model system.

Design and characterization of organelle-targeted RhoA-2 FRET biosensors

An enhanced RhoA sensor was developed for this study by replacing enhanced CFP (eCFP) with mCerulean3 (Figure 1.12A) [52]. Underhill et al. showed that the addition of the brighter CFP mCerulean3 increased the FRET emission activity (unpublished). Using the targeting motifs in Table I, we designed and characterized the targeted RhoA reporters. The proper targeting of RhoA-2 sensors was confirmed as

described above for the respective AKAR4 sensors. MitoRhoA-2 colocalized with MitoTracker (Figure 1.13A) and was enriched in crude mitochondrial fractions (Figure 1.13B). The GolgiRhoA-2 sensor co-localized with the *cis*-Golgi marker GM130 (Figure 1.14A) and did not distort normal morphology of the Golgi apparatus. Isolation of Golgi microsomes followed by western blot analysis further demonstrated that the targeted GolgiRhoA-2 sensors were enriched in these fractions indicating proper targeting of the sensors (Figure 1.14B).

We also generated RhoA sensors targeted to synaptic vesicle (SVRhoA-2) membrane and the nucleus (NuclearRhoA-2). The NuclearRhoA-2 sensor colocalizes with DAPI in transiently transfected SK-N-SH cells (Figure 1.15A). The expression pattern of the targeted SVRhoA-2 sensor in SK-N-SH cells (Figure 1.15B) is reminiscent of classic synaptic vesicle puncta [55].

RhoA activation in response to AMPH favors the ER and Golgi compartments

The targeted RhoA-2 FRET sensors enabled us to assess RhoA activation to AMPH in different subcellular compartments including in the Golgi, mitochondria, ER, nucleus and synaptic vesicle compartments in HEK293 (Figure 1.16A) and SK-N-SH neuroblastoma cells (Figure 1.17A). Baseline FRET emissions for all RhoA sensors were stable (Figure 1.16B). In SK-N-SH (Figure 1.16B, C) and HEK293 cells (Figure 1.15C, D), the FRET sensors exhibited preferential AMPH mediated RhoA activation at the Golgi, and ER membranes compared to mitochondrial, nuclear and synaptic vesicle sensors.

RhoA activation in TAAR1 Knockout (KO) Cells

Previous studies using the untargeted RhoA-2 sensor in wildtype SK-N-SH and TAAR1 KO cell lines have indicated that AMPH-induced RhoA activation is dependent upon TAAR1 activation (unpublished). Similarly, in SK-N-SH cells lacking TAAR1, AMPH stimulation of RhoA is attenuated in almost all organelle compartments (Figure 1.18A; B7). In the absence of TAAR1, AMPH-induced RhoA activation is significantly reduced in the Golgi, ER, nuclear and synaptic vesicle compartments; however, there is no significant difference in RhoA activation in the mitochondrial compartment (Figure 1.18B). These data suggest that the functional site of $G\alpha_{13}$ coupled TAAR1 receptors is localized near the perinuclear membrane compartments of the ER, Golgi.

DISCUSSION

The subcellular localization of TAAR1 determines its availability for its ligands including amphetamine (AMPH) [12,56]. The data presented here provides evidence that TAAR1-mediated PKA and RhoA activation in response to AMPH occurs in distinct compartments of the SK-N-SH neuroblastoma cell line. AMPH entry into the cell requires the DAT [19]. In the cell, AMPH activates TAAR1, which leads to increased PKA and RhoA signaling. Unpublished data from the Amara lab suggests that TAAR1-dependent activation of PKA and RhoA is accomplished through activation of $G\alpha_s$ and $G\alpha_{13}$ coupled TAAR1 receptors, respectively. Elevated RhoA and PKA signaling in response AMPH reciprocally regulate the internalization of DAT and EAAT3 transporters and requires TAAR1 [19]; RhoA activation enhances transporter internalization, whereas PKA signaling decreases RhoA activation and inhibits internalization. In the brain, TAAR1 is co-expressed with DAT and EAAT3 in a subset of DA neurons in the VTA and SN—areas in the brain that have been implicated in drug addiction. DAT and EAAT3 function to regulate synaptic neurotransmitter levels. Therefore, TAAR1-dependent effects of AMPH on DAT and EAAT3 demonstrate that TAAR1 modulates monoaminergic activity in the brain.

The observation of TAAR1's intracellular localization compelled researchers to seek to and identify the membrane localization of TAAR1. Due to limitations of immunolabeling and inconclusive overexpression studies with TAAR1 and its chimeras, the subcellular and functional localization of TAAR1 has not been demonstrated in a neuron. To address this issue, we hypothesized that the use of PKA and RhoA-based

FRET reporters might help to delineate the subcellular and functional localization of TAAR1 using AMPH as a ligand.

Selectively targeted PKA and RhoA-based FRET sensors using organelle-specific targeting motifs were designed and characterized. The Mito-AKAR4 and MitoRhoA-2 sensors localized to the cytoplasmic face of the mitochondria as evidenced by peripheral colocalization with MitoTracker, indicating that the mitochondrial reporters are accessible for activation by PKA and/or RhoA guanine nucleotide exchange factors. The activation of Mito-AKAR4 by dbcAMP a cAMP analog that activates cAMP-dependent protein kinases, is consistent with other previously reported mitochondrial targeted PKA sensors [41]. Golgi-AKAR4 and GolgiRhoA-2 targeted sensors, colocalized with the *cis*-Golgi marker GM130. Nuclear and synaptic vesicle targeted PKA and RhoA reporters were all functional as indicated by increased FRET emission in response to pharmacological activators. Note, that the nuclear reporter was not targeted to the nuclear outer membrane because it is contiguous with the ER membrane. The activity of the lipid-raft and non-membrane raft targeting AKAR4 sensors and the ERRhoA-2 sensor previously developed and characterized by the Zhang and Amara laboratories, respectively were consistent with previously reported findings.

Our results suggest that we can use targeted sensors to identify the subcellular regions where AMPH activates PKA and RhoA pathways and begin to address the compartment(s) where TAAR1 signaling occurs. In SK-N-SH cells, PKA activation significantly favors the synaptic vesicle compartment, however, in HEK293 cells the increase PKA activity in response to AMPH has a broader more diffuse distribution

within the cell. Together with the results of previous studies, these findings suggest that the dynamic localization of PKA and other upstream signaling molecules in this pathway, perhaps through mechanisms involving AKAP proteins, allows for compartmentalization of cellular activities. The absence of synaptic vesicles in HEK293 cells may account for the absence of differential SV–AKAR4 activation in these cells. However, SK–N–SH cells express VMAT₂ and small synaptic vesicles reminiscent of neuronal synaptic vesicle. The robust level of TAAR1–mediated PKA signaling in response AMPH near synaptic vesicles is supported by evidence from several labs suggesting that TAAR1 can regulate monoamine uptake through DAT in striatal synaptosomes and the VTA [10,13,14]. For example, ectopic expression TAAR1 has been shown to increase the extracellular levels of neurotransmitter DA, and NE in the NAc and of serotonin in the medial PFC as evidenced by spontaneous firing rate of monoaminergic neurons in the VTA, dorsal raphe nucleus, and locus coeruleus [10]. However, TAAR1 regulation of vesicular transport and storage has not been demonstrated. Consistent with our results suggesting that TAAR1 maybe be localized in or near synaptic vesicles, immunolabelling studies in thyroid tissue show that secretory vesicles in thyrocytes are immunopositive for TAAR1 [12]. Further studies using TAAR1 KO cells will be needed to confirm TAAR1 localization to the synaptic vesicle compartment in the neuron.

Evidence for TAAR1 localization to the ER and Golgi is also consistent with immunolabelling studies in thyrocytes [12]. Consistent with this, TAAR1–mediated RhoA signaling in response to AMPH is favors the endoplasmic reticulum (ER) and Golgi compartments of SK–N–SH and HEK293 cells. This conclusion is based on

several lines of evidence. First, AMPH treatment in cells transfected with the Golgi and ER-RhoA-2 sensors led to a robust and significant increase RhoA-2 FRET emission compared to all other compartments (Figure 1.17 B–C). In the absence of TAAR1, RhoA activation by AMPH was significantly attenuated in the Golgi and ER compartments (Figure 1.18B). This signal was not completely abolished (Figure 1.18B) suggesting one of two possibilities: 1) TAAR1 may not be the only receptor mediating AMPH-induced RhoA activation and signaling or 2) a certain RhoA baseline activity is relevant even in the TAAR1 KO cell line. Worthy of note, the latter may explain why there was no observed difference in RhoA FRET activity in the mitochondrial compartment between the cell lines (Figure 1.18B). To resolve this full vehicle controls should be used.

The ability of the TAAR1 receptor to couple to different signaling pathways that display distinct spatial and temporal properties is supported by the fact that the downstream components of these pathway are also distinct and can differ in their distribution and kinetics [24]. Taking together, differential PKA response at the synaptic vesicles along with preferential RhoA activation in the Golgi and ER components further confirm that there may be two pools of TAAR1 receptors (unpublished). Our data suggests that $G\alpha_s$ coupled TAAR1 receptors maybe positioned near the synaptic vesicles where they may mediate monoamine storage and release and $G\alpha_{13}$ coupled TAAR1 receptors are localized near the ER/Golgi compartments.

Future studies will seek to further expand our understanding of the downstream effects of AMPH on TAAR1 signaling and defining the membrane localization of TAAR1 in neurons. Commonly used methods such as, subcellular fractionation of

subcellular membrane compartments could provide a static glimpse of TAAR1 trafficking. Developing a TAAR1 antibody for western blot analysis of isolated ER, Golgi and synaptic vesicle membranes fractions may allow us to confirm that TAAR1 is differentially localized to these membrane compartments. Additionally, we can also address whether $G\alpha_{13}$ proteins colocalize with TAAR1 at the ER and Golgi membranes by immunolabelling.

To delineate the functional significance of increased $G\alpha_s$ PKA signaling in the synaptic vesicle compartment we will further characterize the SV-AKAR4 sensor using, immunolabelling and sucrose gradient centrifugation, and explore the possible role of TAAR1 activation in vesicular transport (See Chapter II). As $G\alpha_s$ -cAMP-PKA signaling is highly dynamic, we may need to employ other sensors upstream of the activated protein kinase A-AKAP interaction. Calcium and cAMP may both be required for PKA activation [29] and the use of a cAMP and calcium sensors may assist us in further characterizing the signaling compartment used by TAAR1. Dual FRET imaging could be used to assess AMPH evoked changes in calcium and PKA activity, as used by Dunn et al. to determine the specific roles of various ACs and PDEs in calcium-dependent activation of the cAMP/PKA signaling [29]. A more holistic view of these signaling cascades may be explored with targeted sensors to other cellular compartments including the lysosome, peroxisome and endosome.

In summary, we have designed and characterized new subcellular compartment targeted FRET sensors for use in identifying the functional site of TAAR1-mediated PKA and RhoA activation in response to AMPH. This method provides a means to

explore how coupling of intracellular TAAR1 to different G-protein subunits results in different spatial and temporal patterns of downstream signaling. Using these sensors, we found that $G\alpha_{13}$ coupled TAAR1 receptors responsible for AMPH induced RhoA activation display most robust activation of RhoA with sensors targeted to ER/Golgi compartments while the $G\alpha_s$ coupled TAAR1 receptors responsible for PKA activation appear to generate signals that more prominent in or near the synaptic vesicle membrane. Better antibodies specific for identification of TAAR1 in the neuron are required to establish the precise membrane distribution of TAAR1. As TAAR1's location in the cell determines its availability to ligands including AMPH and METH it is necessary that we determine TAAR1's membrane localization [56]. As new tools to study TAAR1 are developed we can look forward to expanding our understanding of the physiological effects of AMPH on TAAR1 signaling towards delineating the dynamic localization and pharmacokinetic properties of TAAR1 in both therapeutic and addictive actions of psychostimulant drugs [24].

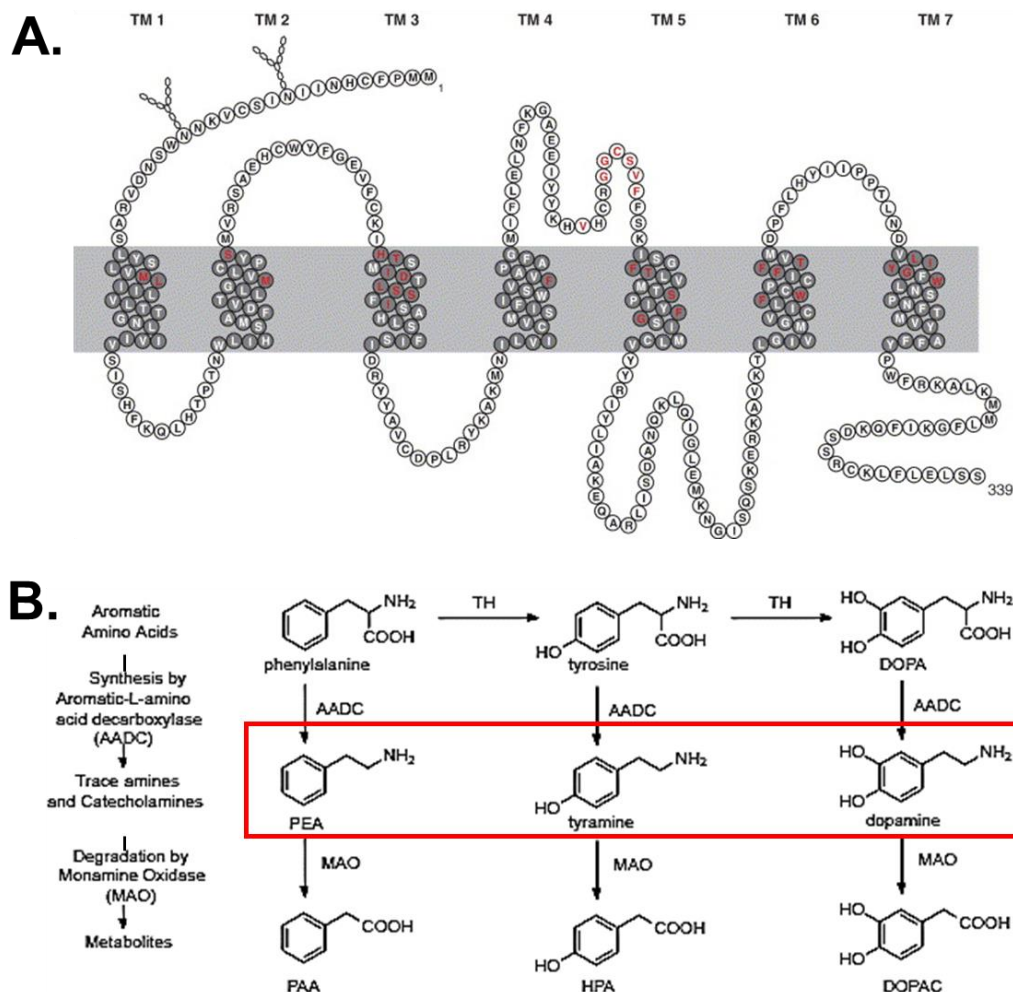


Figure 1.1| TAAR1 structure and ligands. (A) Predicted model of the transmembrane topology of the human trace amine associated transporter 1 (*hTAAR1*). TAAR1 is a seven transmembrane (TM) G-protein coupled receptor. The gray shaded amino acid residues in the TM domains are phylogenically conserved. Putative N-terminal glycosylation sites at asparagine residues N10 and N17 should confer localization to the plasma membrane; however, TAAR1 is predominantly localized intracellularly and the N-terminal glycosylation sites may govern activity dependent TAAR1 membrane localization [57,58]. Image was adapted from Lindemann et al. 2008 [9]. (B) Trace amines share similar structural, and metabolic pathways as the neurotransmitter dopamine. The enzyme aromatic-L-amino acid decarboxylase (AADC) is necessary for the conversion of aromatic amino-acids to biogenic amines like DA and for generating endogenous trace amines (TAs). The most potent trace amine, ρ -tyramine is formed from the tyrosine substrates, while β -PEA is formed from phenylalanine. The absence of MAO increases the half-life and account for physiological effects of TAs seen in patients with *tyramine storm* [3,5,6,59].

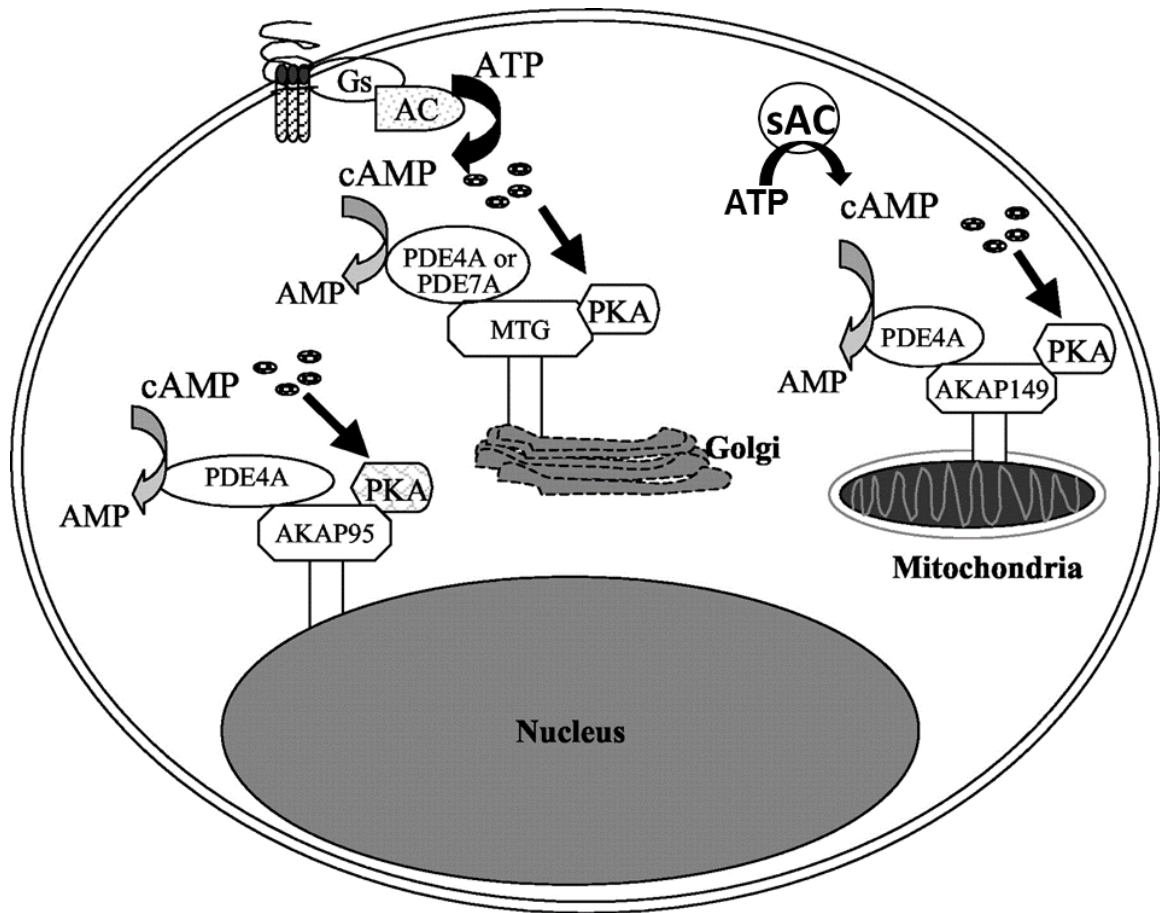


Figure 1.2| Subcellular targeting of PKA signaling through AKAPs. AKAPs target PKA, along with its substrates and regulators to form a complex at specific organelle compartments, for example, mitochondria, Golgi, and nucleus. The binding of AKAPs to specific partners, such as phosphodiesterase (PDE) regulates the activation and deactivation of PKA signaling. Activation of $G_{\alpha s}$ coupled GPCRs turns on soluble and/or plasma membrane bound adenylyl cyclases (sACs; pmACs) resulting in elevated formation of intracellular cAMP from ATP. Four cAMPs then bind to regulatory subunits of PKA leading to the activation of PKA. PDE locally promote rapid inactivation of cAMP to AMP and dephosphorylation of PKA substrates. AKAP350 (Golgi), D-AKAP1 (mitochondria), and AKAP95 (nucleus) tethers PKA and compartment specific PDE and AC which together act to maintain cAMP homeostasis in each microdomain of the cell [32]. This image was modified from Asirvatham et al. 2004 [32].

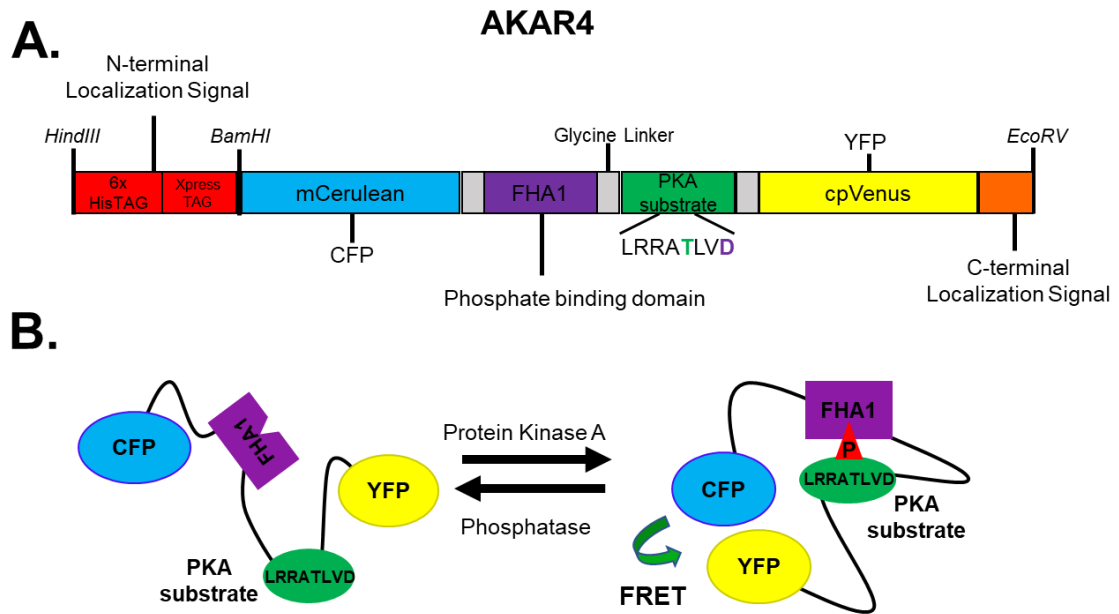


Figure 1.3| A–Kinase Activity Reporter 4 (AKAR4) FRET biosensor. (A) *Schematic of AKAR4, a PKA–based Intramolecular FRET reporter.* The AKAR4 plasmid construct of the intramolecular PKA biosensor consists of the phosphoamino–acid–binding domain of the forkhead associated protein 1 (FHA1, purple), which selectively binds to the phosphorylated PKA substrate (LRRATLVD, green). In the target PKA substrate motif sequence, the characters labelled in green and purple indicate the residues for phosphorylation, and FHA1 binding respectively. The phosphate binding domain is separated from the donor cyan fluorescent protein, mCerulean (CFP, blue) by a glycine linker. Another glycine linker separates the yellow fluorescent protein variant, cpVenus (YFP) from the PKA substrate [41,42]. The PKA substrate is separated from cpVenus by another glycine linker. The organelle targeting sequence motifs were added to the N–or C–terminal of the AKAR4 plasmid using the restriction sites indicated. Schematic was adapted from Depry et al. 2011 [42]. (B) *Mechanism of Intramolecular PKA–FRET.* Phosphorylation of the surrogate PKA substrate by PKA promotes the association of the FHA1 domain to the substrate, inducing a conformational change, which brings the donor CFP and YFP closer together resulting in an increased FRET emission. The diagram in B was adapted from Komatsu et al. 2011 [43].

Table I| Targeting motifs. The targeting motifs were fused to the AKAR4 and RhoA–2 FRET–based reporters. The nontargeted AKAR4 plasmid was obtained as a gift from Zhang laboratory [42]. The asterisk (*) indicates that these plasmids with these targeting motifs were designed and generated prior to this study. The targeting motifs of Lyn, Kras and ER were added to AKAR4 by the Zhang laboratory and were also acquired as gifts [42,60]. These three motifs were also added to the RhoA–2 FRET sensor prior to this study by the Amara lab (unpublished).

Name	Localization	Targeting Sequence Position	Origin	Amino Acid Sequence	Citations
Nuclear	Nucleus	C–terminus	Human cMYC proto–oncogene;	PAAKRVKLD	[46]
Nuclear	Nucleus	C–terminus	SV40 Large T antigen	PKKKRKVEDP	[46]
Mito	Outer mitochondrial membrane	N–terminus	D–AKAP1	MAIQLRSLFPLALPGMLALLGWWWF FSRKKDP	[49,50]
Mito	Outer mitochondrial membrane	N–terminus	Tom20	MVGRNSAIAAGVCGALFIGYCIYFDR KRRSDPNNGGGGGGGGGDP	[51]
Golgi eNOS	Golgi Apparatus	N–terminus	Endothelial nitric oxidase	MGNLKSVAQEPGPPCGLGLGLGLGL CGKQGPATPAGGGGGGGGGDP	[47-48]
Giantin 3131-3529	Golgi Apparatus	C–terminus	Giantin	EPQSFSEAQQQLCNTRQEVNELRKL LEEERDQRVAENALSVAEEQIRRL HSEWDSSRTPIGSCGTQEQALLIDL SNSCRTRSGVGWKRVLRSLSCHSRTR VPLLAAYFLMIHVLLLCFTGHL	[43,51]
SV	Synaptic Vesicle	C–terminus	VMAT2 (Slc18a2)	RSPPAKEEKMAILMDHNCPIKTKMYT QNNVQSYPIGEDEESESD	[53,54]
Kras *	Non–raft plasmid membrane	C–terminus	KRAS GTPase (V–Ki–ras2 Kirsten rat sarcoma viral oncogene homolog)	KKKKKKSKTKCVIM	[42]
Lyn *	Lipid raft	N–terminus	Lyn Kinase (Lck/Yes novel tyrosine kinase)	MGCIKSKRKDKDP	[42]
ER *	Endoplasmic Reticulum	N–terminus	Cytochrome p450	MDPVVVLGLCLLCLLLSLWKQSYG GGDP	[60]

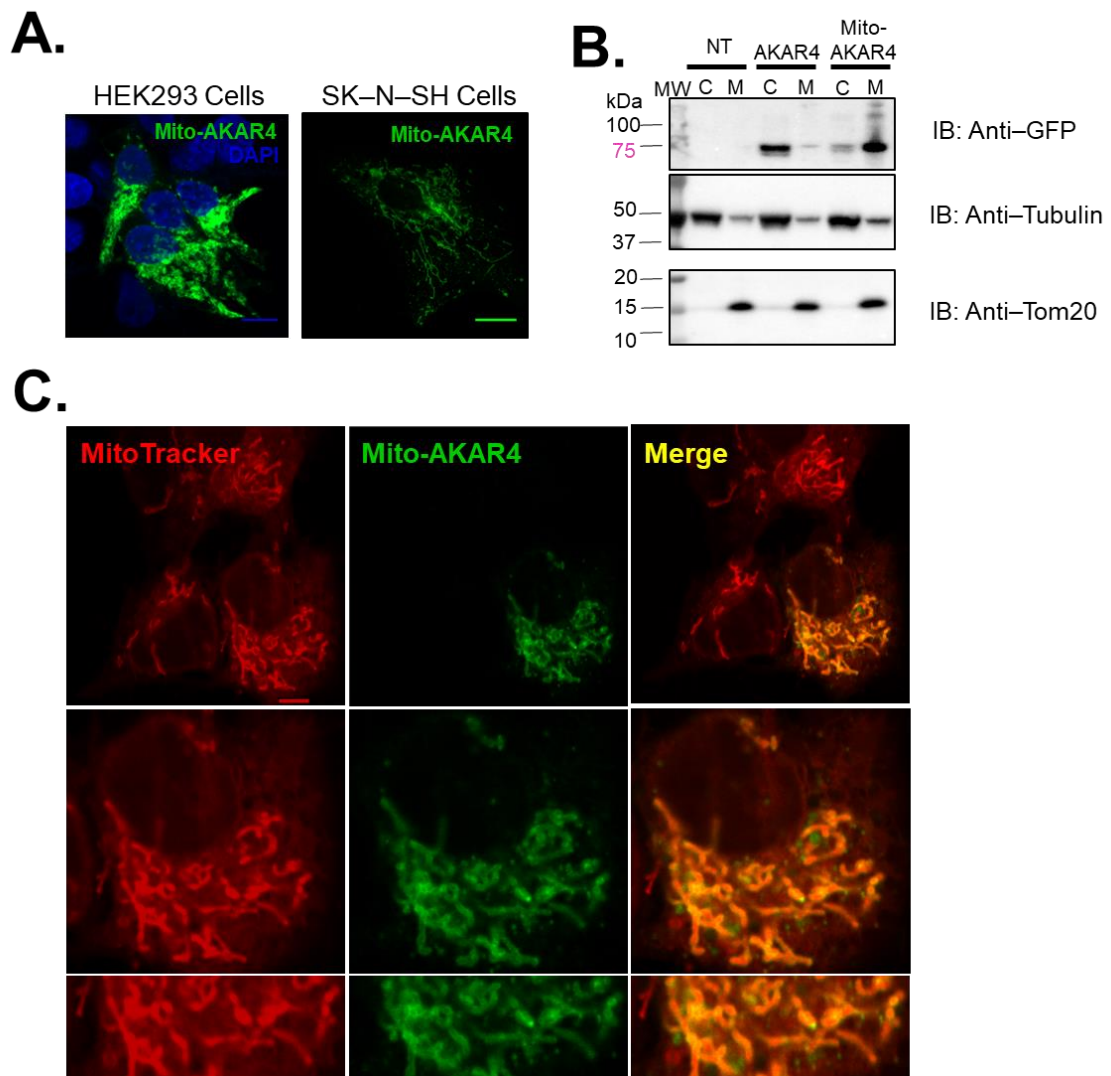


Figure 1.4| Mitochondrial targeting of AKAR4. (A) Confocal images of Mito-AKAR4 in HEK293 and SK-N-SH cells. Mito-AKAR4 (green) and DAPI (nucleus, blue) in HEK293 and SK-N-SH cells. Scale bar, 10 μ m. (B) Mito-AKAR4 is targeted to mitochondrial fractions. HEK293 cells were transfected with Mito-AKAR4 or the non-targeted AKAR4 construct. Mitochondrial fractions were isolated with a mitochondrial isolation kit. Following isolation, the samples were analyzed by western blot for GFP, Tom20 (a mitochondrial marker) and α -tubulin (a cytosolic marker). Non-transfected HEK293 cells were processed in parallel as a negative control. Mito-AKAR4 localizes predominantly to the mitochondrial fraction, M while AKAR4 is found in the cytoplasmic fraction, C. (C) Live cell imaging of Mito-AKAR4 and MitoTracker. Mito-AKAR4 (green) colocalized with MitoTracker (red) and appears at the peripheral and outer membrane of the mitochondria in SK-N-SH cells. Yellow in merge shows colocalization. Scale bar, 10 μ m.

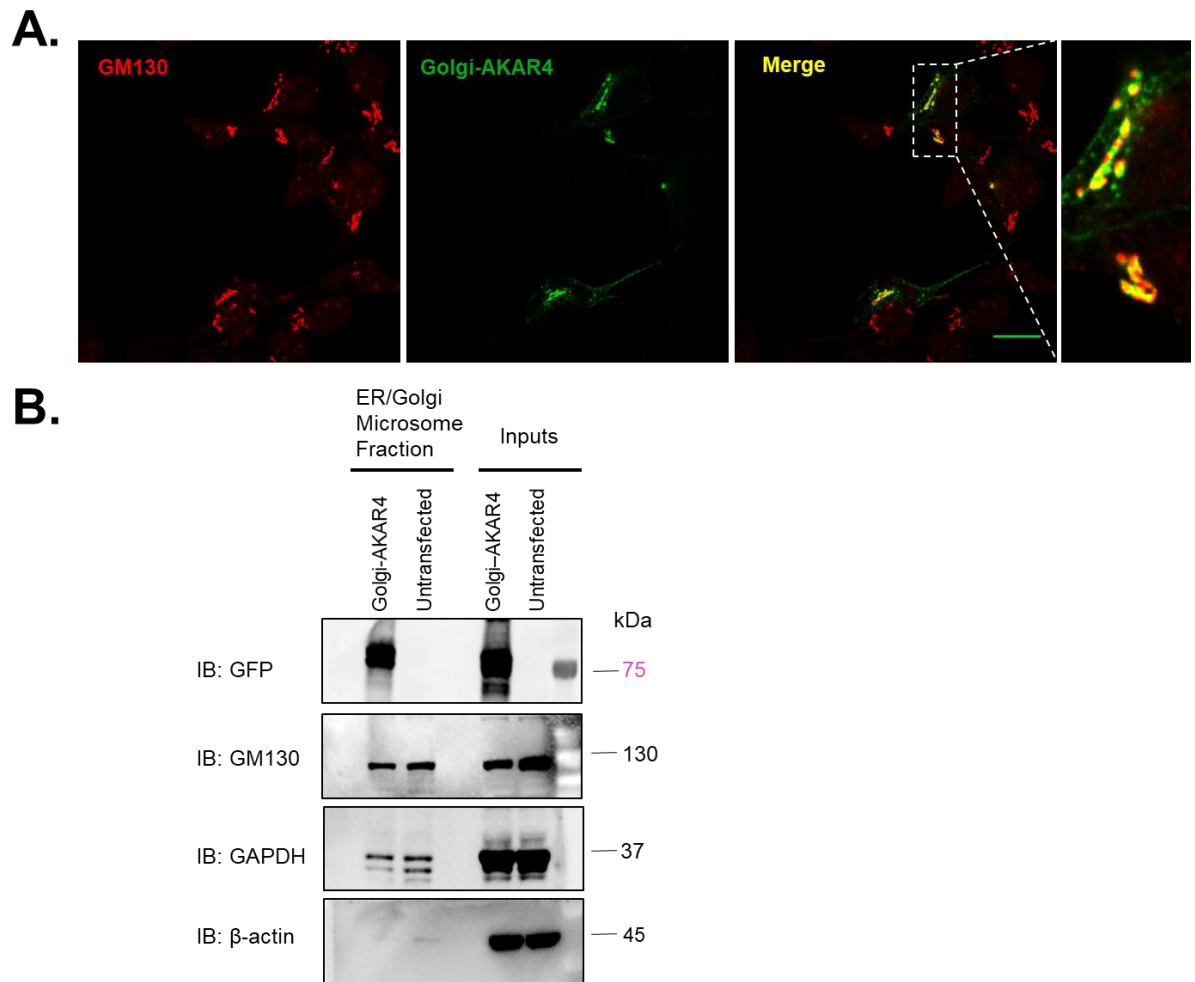


Figure 1.5| Localization of Golgi-AKAR4. (A) *Golgi-AKAR4* colocalizes with *cis-Golgi* marker *GM130*. SK-N-SH cells were transiently transfected with *Golgi-AKAR4* (green) and probed with a *GM130* antibody (red). Scale Bar, 10 μ m. (B) *Golgi-AKAR4* is enriched in *Golgi microsomes*. Crude microsomal preparations of the *Golgi* followed by western blot analysis for GFP further confirms *Golgi-AKAR4* localization. *GM130* (a *Golgi* Marker), β -actin (a cytosolic marker) and *GAPDH* (cytosolic markers) were used as controls for the *Golgi* and cytosolic fractions.

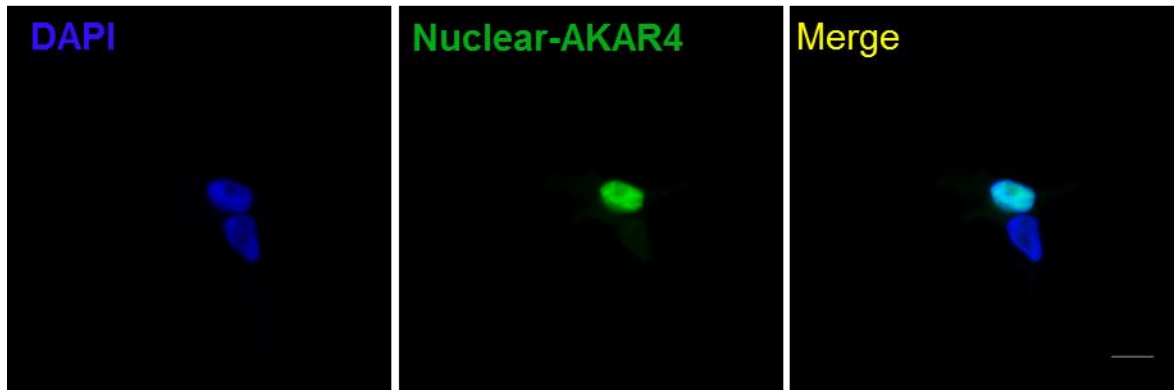


Figure 1.6| Characterization of the Nuclear-AKAR4 biosensor. Nuclear-AKAR4 (green) colocalized with DAPI (blue). Scale bar, 10 μm .

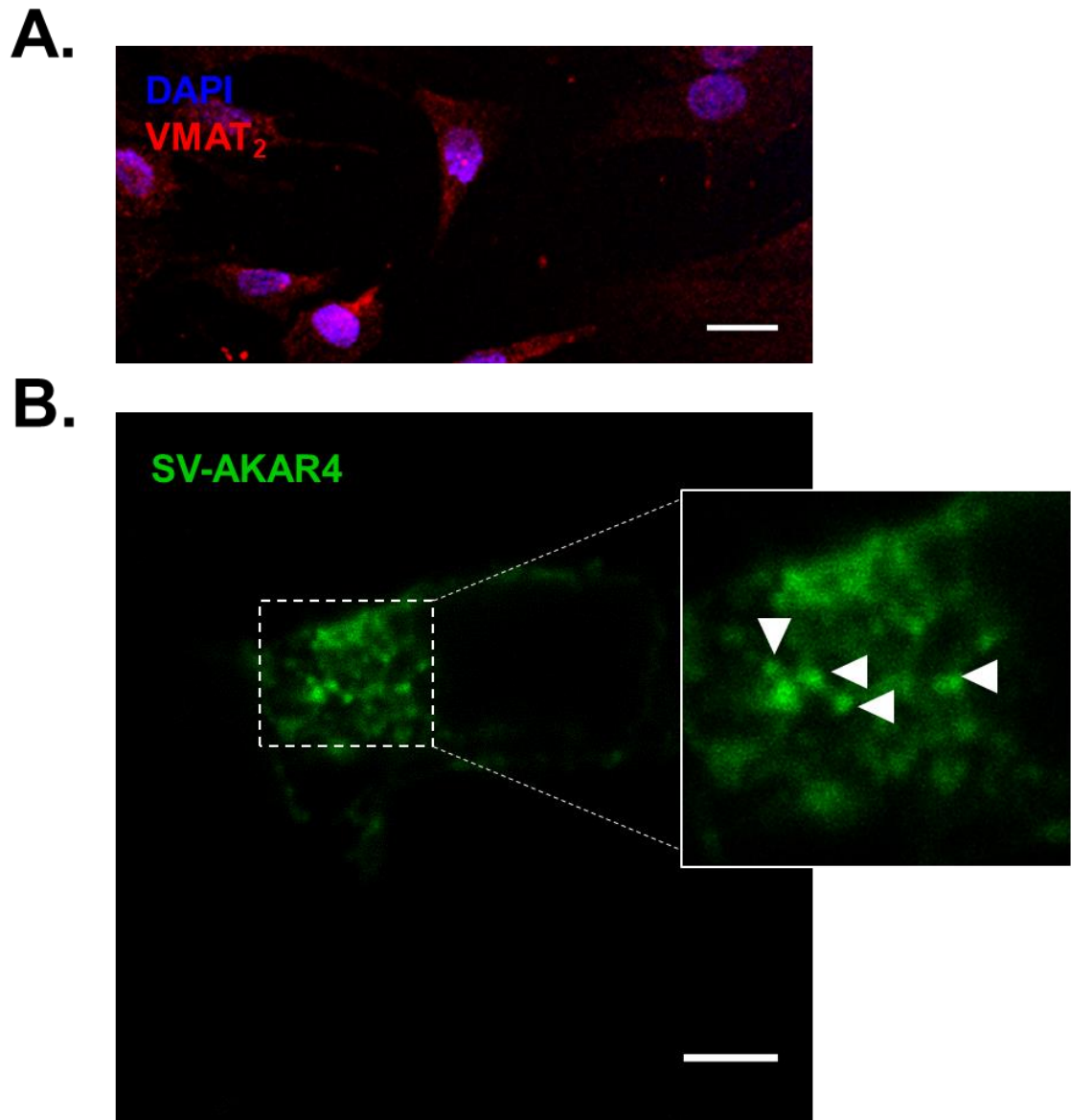
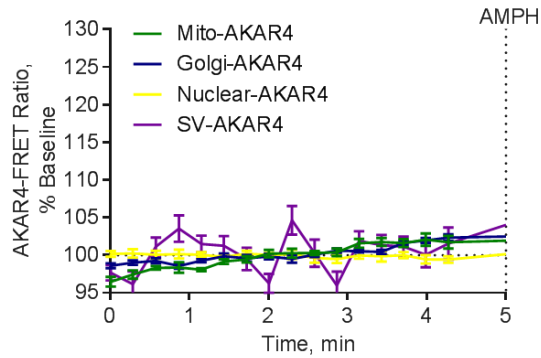


Figure 1.7| Cellular distribution of SV-AKAR4. (A) *SK-N-SH* cells express *VMAT₂*. *SK-N-SH* cells were stained with antibodies to the vesicular monoamine transporter 2, *VMAT₂* (red) and a DNA marker DAPI (blue) stains the nucleus. *VMAT₂* positive staining appears as punctate dots through the cell. Scale bar, 10 μm. (B) *SV-AKAR4* expression profile resembles synaptic vesicle and *VMAT₂*. *SK-N-SH* cells transfected with *SV-AKAR4* show that the sensor has a punctate (white arrow) distribution in the cell similar to *VMAT₂* positive synaptic vesicles. Scale bar, 10 μm.

A. cAMP-mediated PKA Activation, SK-N-SH Cells



B. cAMP-mediated PKA Activation, SK-N-SH Cells

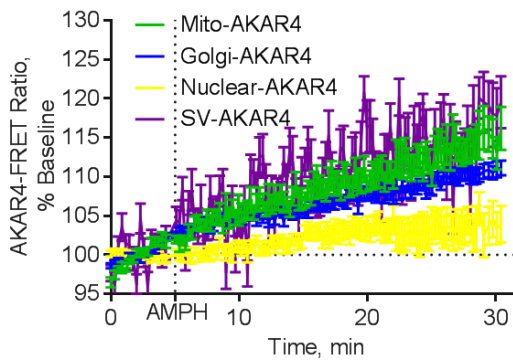


Figure 1.8| Organelle-specific intramolecular PKA biosensors are stimulated by cAMP. (A) Basal PKA activation was steady prior to administration of cAMP analogue *dbcAMP*. Baseline recording of PKA reporters prior to pharmacological activation by *dbcAMP* indicate steady state activation of PKA at 100 %. (B) *dbcAMP* activates targeted AKAR4 sensors. Treatment of SK-N-SH cells expressing the respective AKAR4s led to an increase in FRET emission ratios for all AKAR4 sensors studied. This demonstrates that activation of the PKA enzyme by *dbcAMP* is sufficient to generate changes at distinct microdomains.

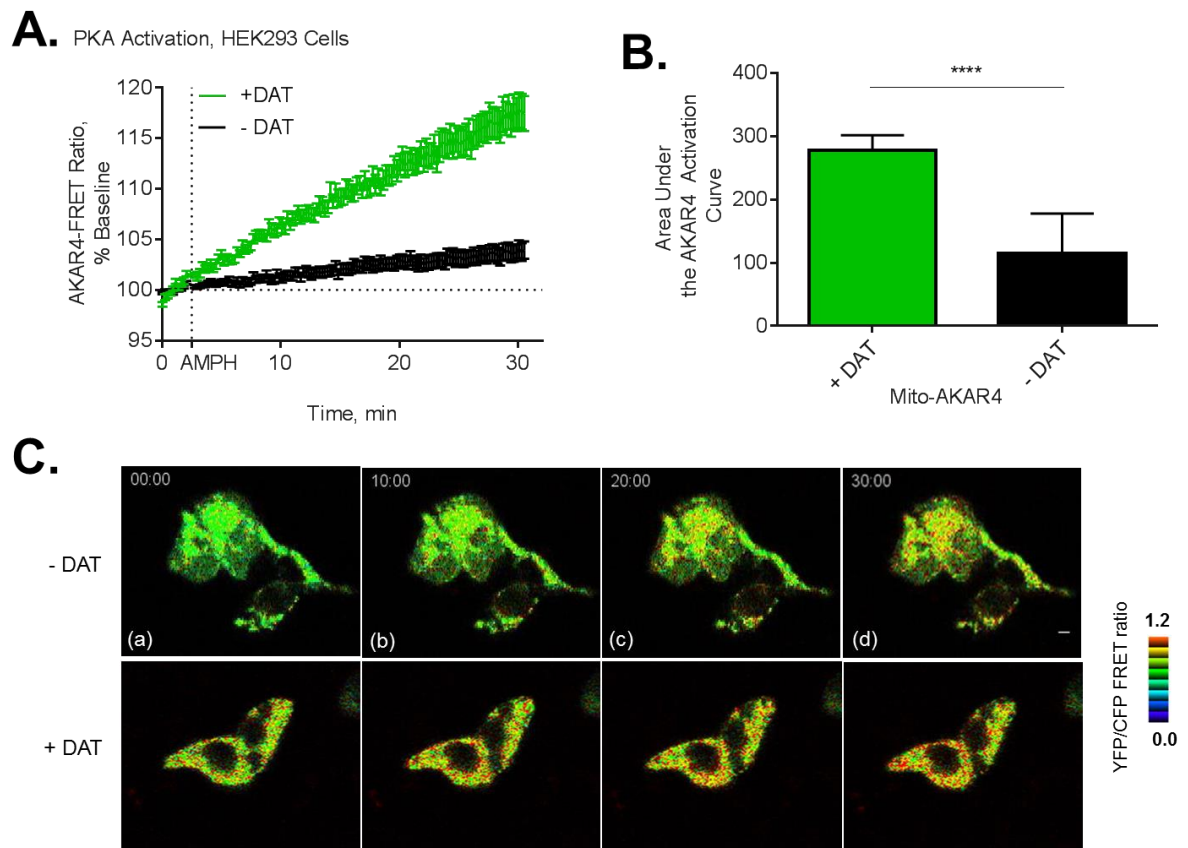


Figure 1.9| AMPH mediated PKA activation requires DAT. (A) HEK293 cells co-expressing Mito-AKAR4 and DAT show increases in PKA activation (green lines). However, in cells that do not co-express DAT, AMPH (10 μ M) treatment did not result in marked increased in PKA activation (black lines). This DAT-dependence is consistent with previously published data [10,13,19,21]. Maximum change in FRET emission ratio at 30 minutes was 117.45 ± 1.73 % for cells transfected with both DAT and Mito-AKAR4 compared to 103.95 ± 0.85 % in the absence of DAT. (B) Analysis of the AUC indicates that AMPH-mediated PKA activation in the presence of DAT is significantly greater than without DAT co-expression. (**** $p \leq 0.0001$ by two-tailed parametric t-test). (C) Representative single cell images of the FRET emission ratio changes in HEK293 cells. Top FRET YFP/CFP emission ratio in the absence of DAT and bottom FRET YFP/CFP in the presence of DAT at various time points. Scale bar, represents 10 μ m.

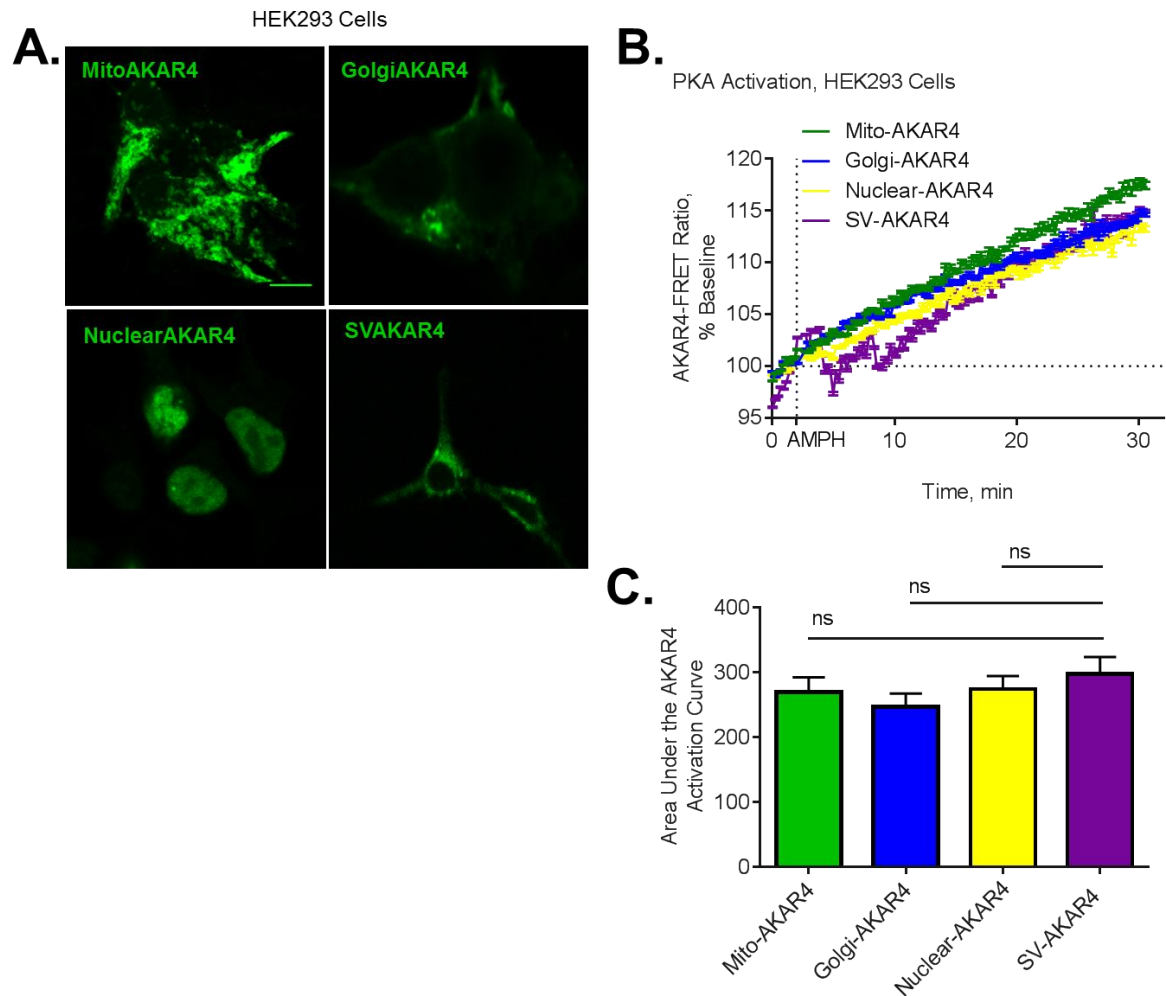


Figure 1.10| PKA–FRET biosensors do not show preferential responses to AMPH in HEK293 cells. (A) HEK293 cells expressing the four targeted AKAR4 sensors to the mitochondria, Golgi and synaptic vesicle membranes and the nucleus showed canonical localization and organelle morphology. (B) PKA activation by AMPH was detected in all organelle compartments. (C) Analysis of the area under the curves (AUC) followed by one-way ANOVA analysis compared to SV–AKAR4 showed no significant difference in activation by AMPH. (ns, statistically nonsignificant).

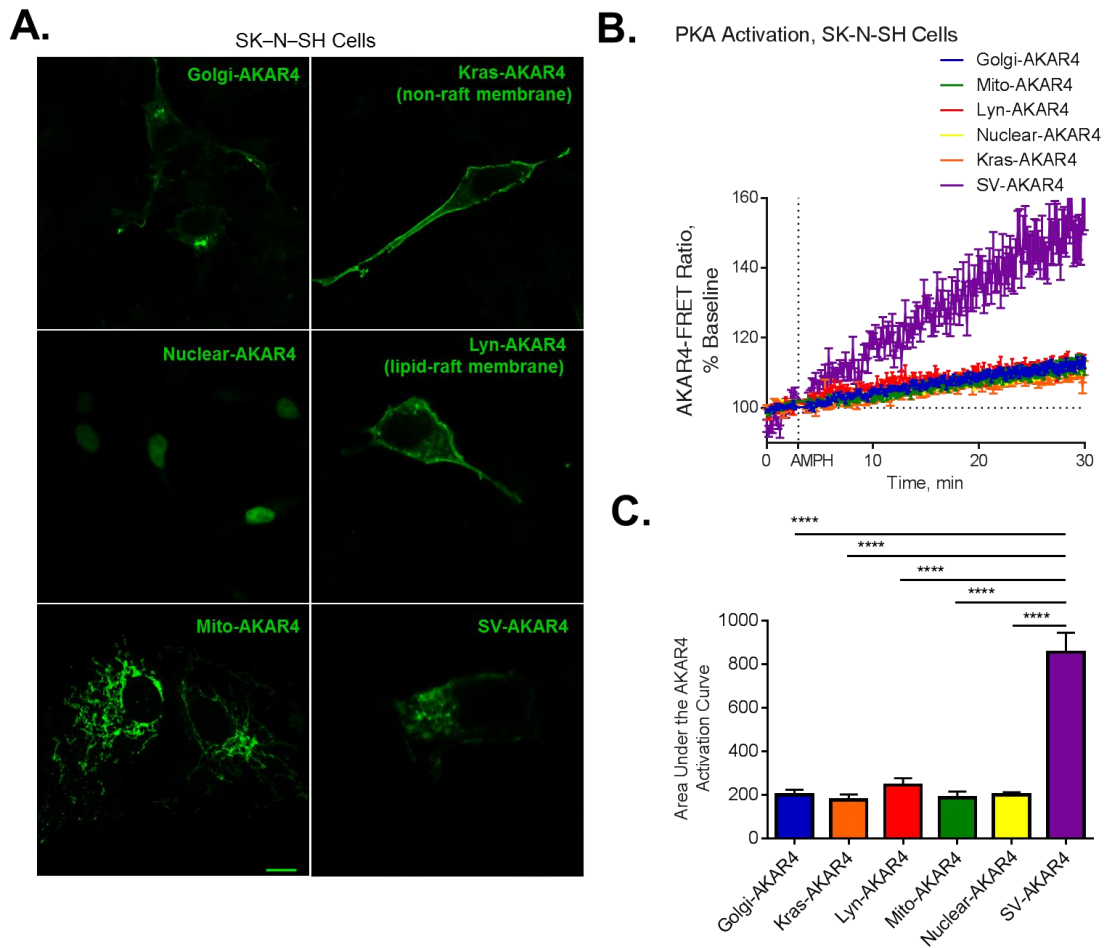


Figure 1.11| PKA activation in response to AMPH favors synaptic vesicles in SK-N-SH cells. (A) SK-N-SH neuroblastoma cells co-transfected with DAT and different targeting AKAR4 sensors. The biosensors targeted to the mitochondria Golgi, synaptic vesicle, lipid-raft and non-raft membranes and the nucleus show canonical localization and organelle morphology. (B) PKA activation by AMPH was detected in all organelle compartments. (C) Analysis of the AUC followed by one-way ANOVA analysis indicate that the synaptic vesicle targeted (SV-AKAR4, purple) PKA sensor is significantly activated in response to AMPH compared to all other compartments (**** $p < 0.0001$).

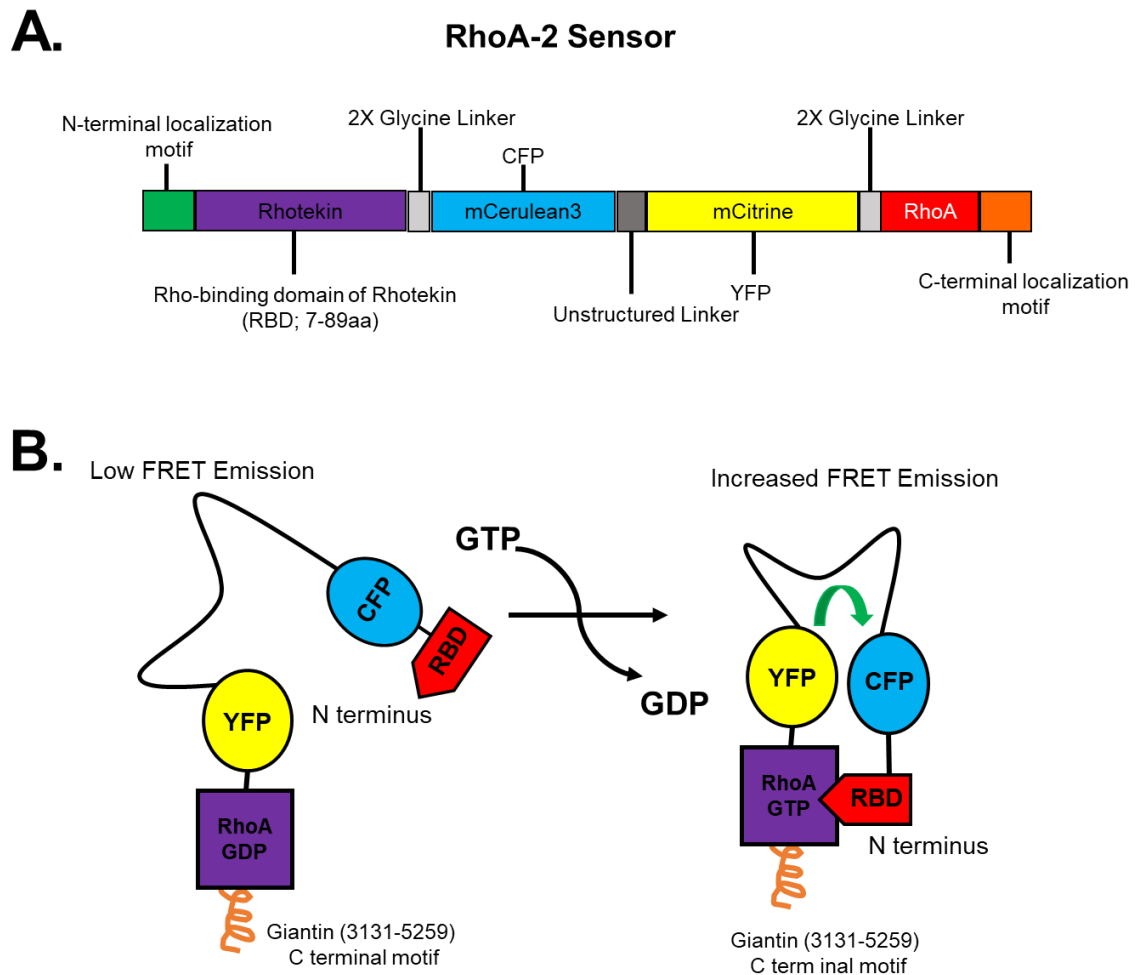


Figure 1.12 | RhoA-2 FRET biosensor. (A) *Schematic of RhoA-2, a Rho-based intramolecular FRET sensor.* The RhoA-2 plasmid construct for the intramolecular RhoA biosensor consists of the Rho-binding domain (RBD) of rhotekin, which binds to GTP-bound RhoA GTPase. The Rho-binding domain is separated from the donor CFP variant, mCerulean3 by a 2X glycine linker. mCerulean3 (blue) is a brighter third generation fluorophore [45]. An unstructured linker separates the acceptor YFP variant, mCitrine from mCerulean3 [45]. The mCitrine is separated from full length RhoA protein by another 2X glycine linker. The organelle targeting sequence motifs were added to the N- or C-terminus of the RhoA-2 plasmid. (B) *Mechanism of intramolecular RhoA-2 FRET emission.* Conversion of inactive GDP-bound RhoA to activated GTP-bound RhoA by guanine exchange factors promotes the association of rhotekin with RhoA-GTP, inducing a conformational change, which brings the donor CFP and YFP closer together resulting in increased FRET emission. This schematic is based on an original figure from Pertz et al. 2006 [45].

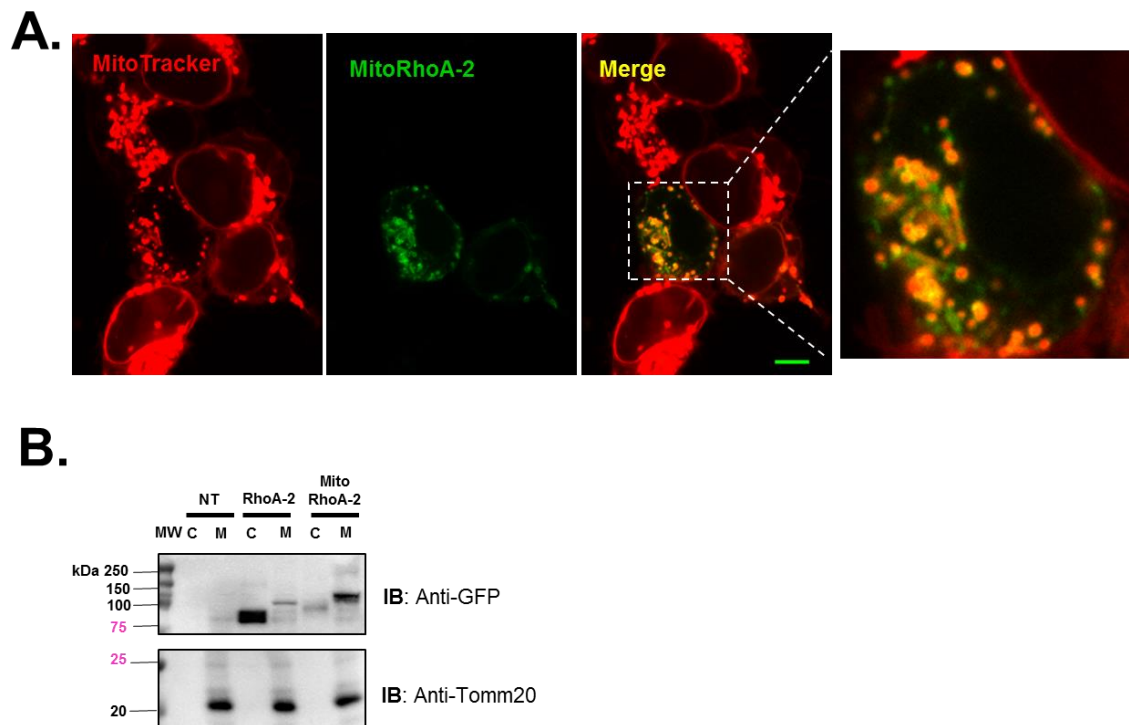


Figure 1.13| Localization of MitoRhoA-2. (A) *MitoRhoA-2* properly localizes to the mitochondrial compartment. In transfected HEK293 cells, MitoRhoA-2 is colocalized with the mitochondria specific dye, MitoTracker (red). Scale bar, 10 μ m. (B) *Mitochondrial fractions are enriched in MitoRhoA-2.* HEK293 cells transiently transfected with the untargeted RhoA-2 plasmid or the MitoRhoA-2 reporter were fractionated and separated by SDS-PAGE gel electrophoresis followed by western blot analysis. RhoA-2 is enriched in the cytoplasmic fractions, C, and absent from the mitochondrial fractions, M. Non-transfected cells were used as a negative control.

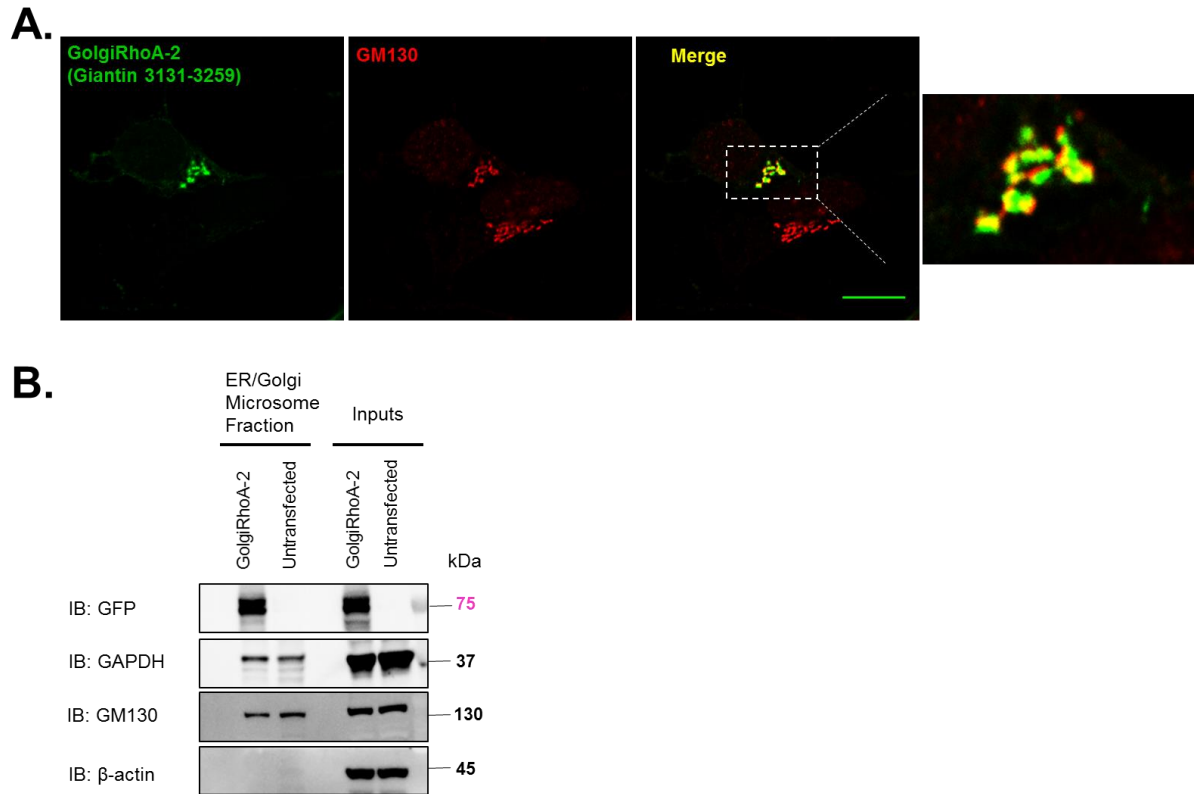


Figure 1.14| GolgiRhoA–2 localizes to the Golgi apparatus. (A) *GolgiRhoA–2* colocalizes with *GM130*. Transiently transfected SK–N–SH cells were fixed and immunostained with the Golgi marker. Scale bar, 10 μ m. (B) *GolgiRhoA–2* is enriched in crude ER/Golgi microsomes. An equal amount of protein (30 μ g per lane) from the ER/Golgi enriched fractions and whole cell lysates (inputs) prepared from HEK293 cells were analyzed by western blot. The purity of ER/Golgi fractions were assessed for the presence of *GM130* (a Golgi marker) and the absence of *GADPH* (A cytosolic marker) and β -actin (a cytosolic marker).

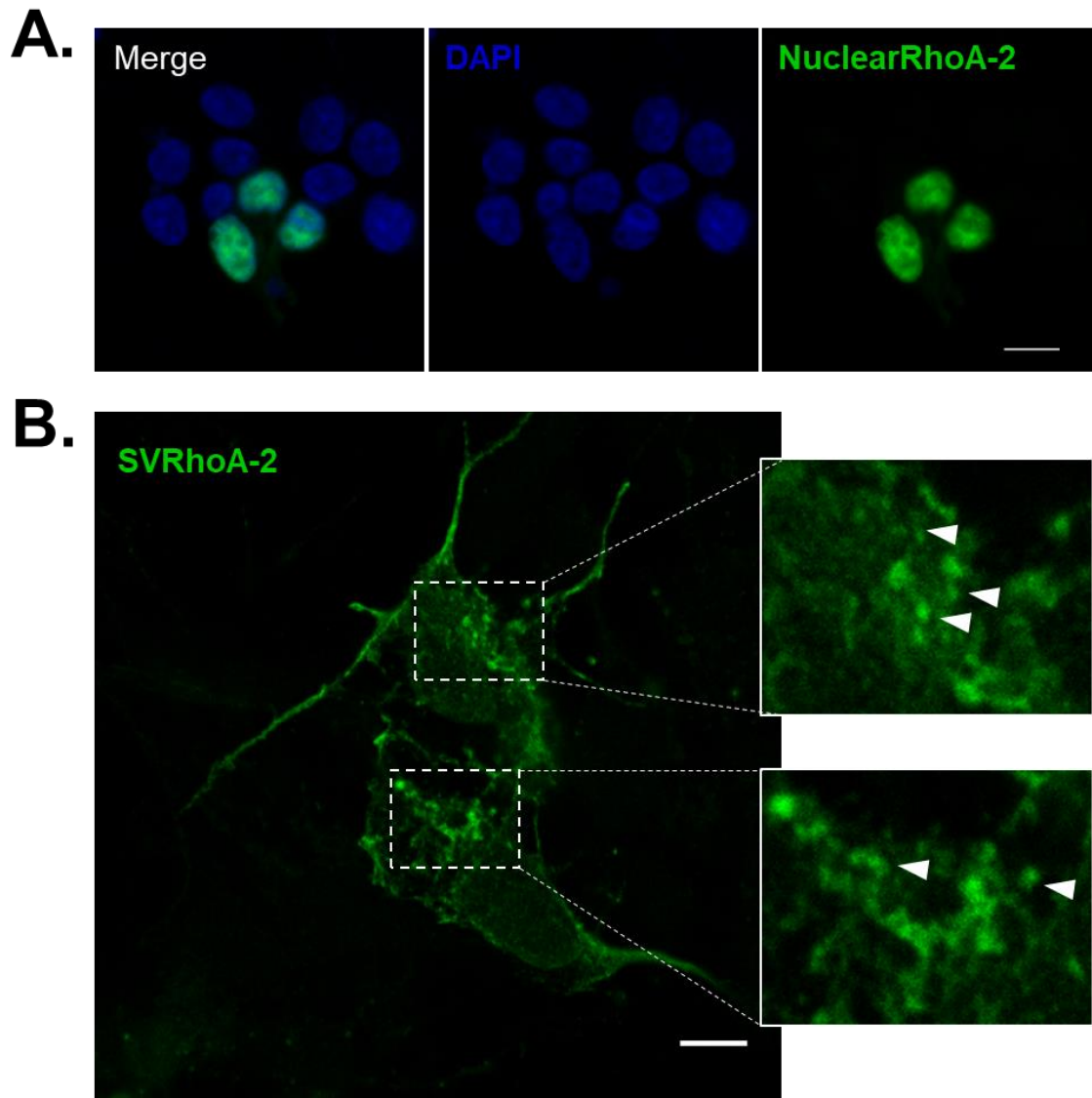


Figure 1.15| NuclearRhoA-2 and SVRhoA-2 cellular distribution. (A) *NuclearRhoA-2* localizes to the nucleus. SK-N-SH neuroblastoma cells transiently transfected with *NuclearRhoA-2* and stained with DAPI. Both *NuclearRhoA-2* (green) and DAPI (blue) co-localize as indicated in the merged image. Scale bar, 10 μm . (B) *SVRhoA-2* expression resembles synaptic vesicle and *VMAT2*. SK-N-SH cells transfected with *SVRhoA-2* (green) indicate that the sensor has a punctate (white arrows) distribution in the cell reminiscent of *VMAT2* positive synaptic vesicles. Scale bar, 10 μm .

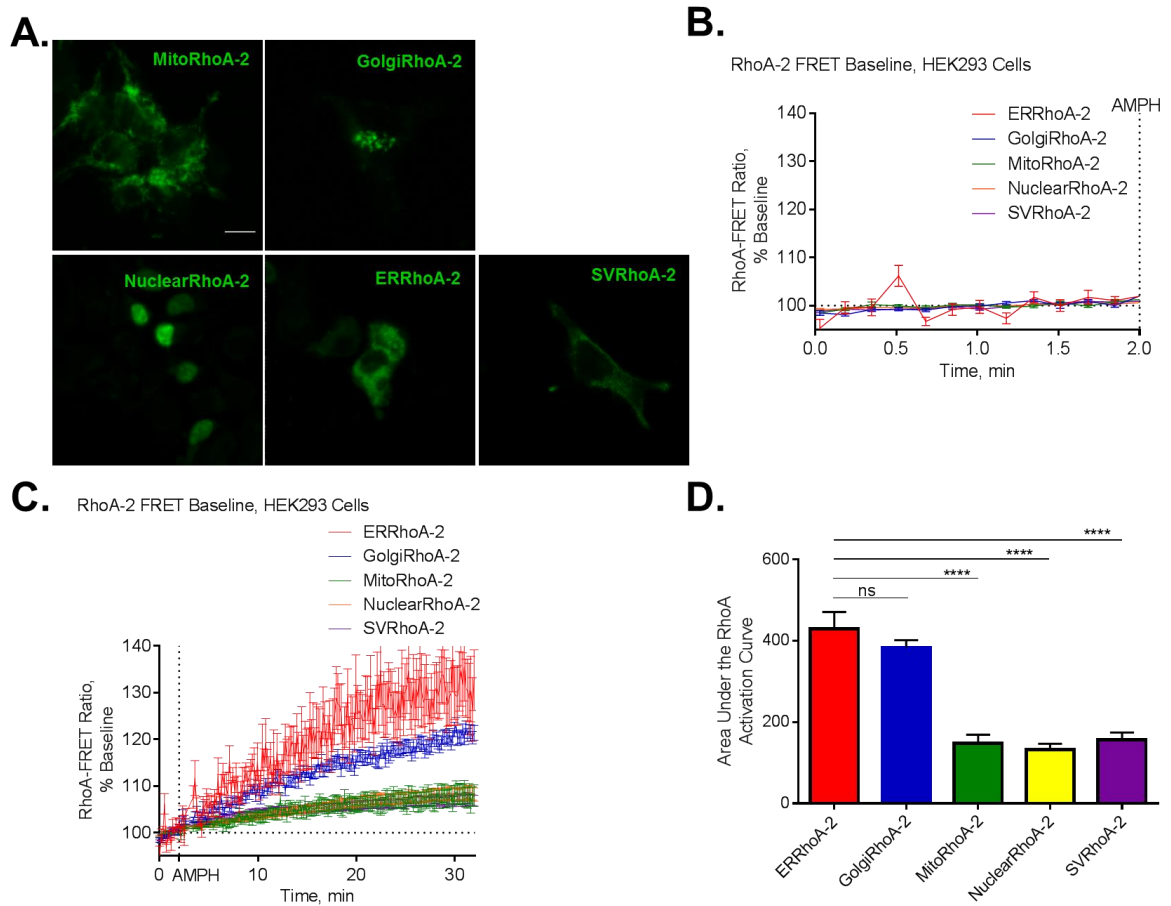


Figure 1.16| RhoA biosensor response to AMPH is most robust in the ER/Golgi membranes in HEK293 cells. (A) HEK293 cells co-transfected with DAT (unlabeled) and different targeting RhoA-2 sensors (green). The biosensors targeted to the mitochondria (MitoRhoA-2), Golgi (GolgiRhoA-2), synaptic vesicle (SVRhoA-2), and endoplasmic reticulum (ERRhoA-2) membranes and the nucleus (NuclearRhoA-2) were localized to the predicted compartments. (B) Steady state RhoA activation. Baseline RhoA-2 responses prior to pharmacological activation by AMPH were stable at 100%. (C) RhoA-2 activation by AMPH was detected in all organelle compartments. HEK293 cells were stimulated with AMPH (10 μ M) at 2 minutes preceding baseline FRET recordings. (D) Analysis of the AUC indicates by one-way ANOVA analysis that the RhoA response to AMPH are greater in the Golgi (blue) and ER (red) compartments. (**** $p < 0.0001$ by one-way ANOVA compared to ER; ns, statistically nonsignificant).

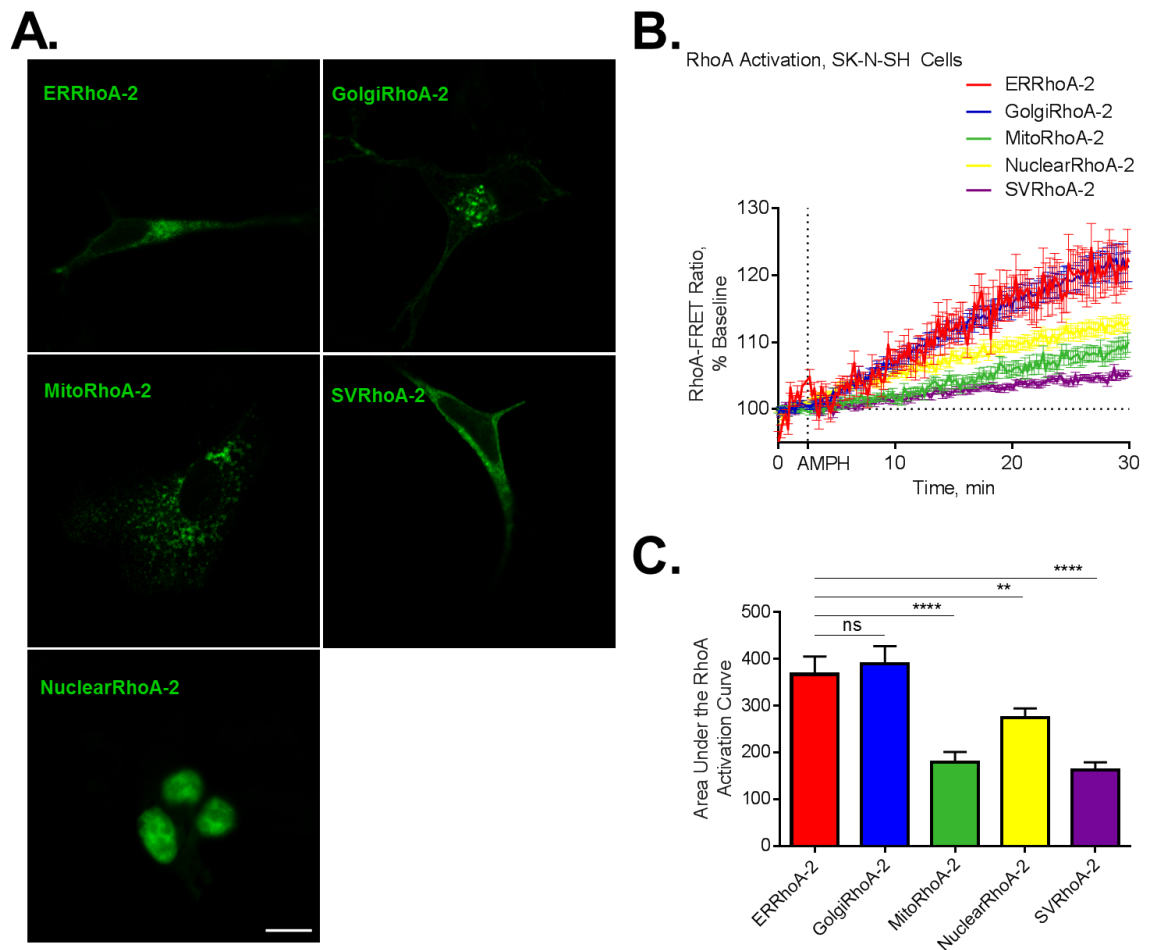


Figure 1.17| AMPH-induced RhoA biosensor activity favors the ER/Golgi domains in SK-N-SH cells. (A) SK-N-SH neuroblastoma cells co-transfected with DAT and different targeting RhoA-2 sensors. All targeted biosensors showed canonical localization and organelle morphology when transfected in SK-N-SH cells. (B) RhoA activation by AMPH was detected in all organelle compartments. SK-N-SH cells were stimulated with AMPH (10 μ M) at 2 minutes preceding basal FRET recordings. (C) AUC analysis indicates that TAAR1-mediated RhoA response to AMPH favors the Golgi (blue) and ER (red) compartments. (** $p < 0.01$ and **** $p < 0.0001$ by one-way ANOVA compared to both ER and Golgi compartments; ns, statistically nonsignificant).

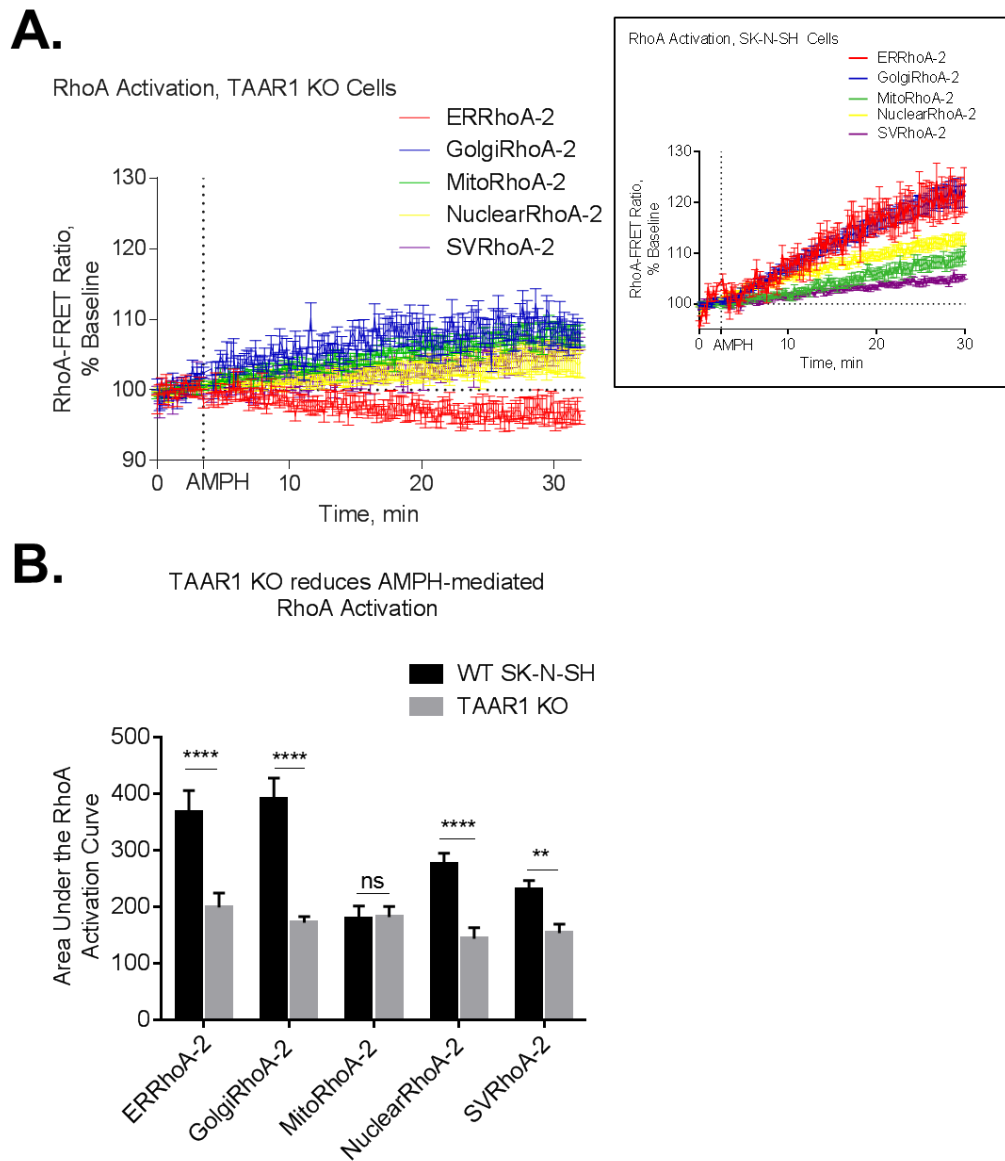


Figure 1.18| RhoA Activation in response to AMPH is attenuated in TAAR1 KO SK–N–SH cells. (A) Representative curves of targeted sensors response to AMPH in TAAR1 KO cells. CRISPR–Cas9 deletion of TAAR1 in SK–N–SH cells reduce AMPH–induced RhoA activation in almost all organelle compartments transfected with DAT and respective RhoA sensors in comparison to wildtype SK–N–SH cells (Inset, from Figure 1.17). (B) Summary of AMPH stimulated RhoA Activation in TAAR1 KO cells. We compared the AUC of WT SK–N–SH cells in Figure 1.17C to data from three separate experiments in TAAR1 KO cells. The absence of TAAR1 significantly reduces RhoA activation response in almost all compartments and is most significant in the Golgi, ER and nuclear compartments.

CHAPTER TWO: INTRODUCTION

VMAT Function and Location

The integrity and strength of monoaminergic neurotransmission requires the coordination of several critical steps, including (1) synthesis of monoamines and their precursors in the cytoplasm; (2) loading of neurotransmitter (NT) synaptic vesicles where they are sometimes further modified; and (3) exocytosis from vesicles into the synapse [61–63]. Dysregulation in any of these steps presents in a myriad of neurological and neuropsychiatric disorders including schizophrenia, Parkinson's and drug addiction [63]. A key determinant of synaptic neurotransmission and function is the availability of monoamines for storage and release by synaptic vesicles. In midbrain dopaminergic neurons, these processes are partly mediated by vesicular monoamine transporter 2, VMAT₂, which belong to the *Slc18* family of cation-dependent neurotransmitter transporters [64,65]. VMAT₂ is a twelve-transmembrane pH and proton-ATPase-dependent transporter responsible for storage and release of DA, serotonin, histamine and norepinephrine in the peripheral and central nervous system (PNS; CNS). For every substrate transported into the vesicle, two protons are pumped from the intravesicular space into the cytoplasm. Vesicular uptake of neurotransmitters prevents rapid degradation of monoamines into toxic metabolites and neurotoxic oxidation [63–66].

VMAT₂ (*Slc18a2*) is structurally-related to VMAT₁ (*Slc18a1*) but the two transporters possess distinct pharmacological properties and distributions [67]. Both isoforms of VMAT are localized to large dense-core vesicles (LDCV) in the PNS. In the

mammalian brain, however, VMAT₂ is present in small synaptic vesicles (SSV) [62,65,68,69]. It is believed that VMAT₁ is preferentially localized to LDCV of neuroendocrine cells in the PNS, while VMAT₂ is thought to localize to both LDCV in the PNS and SSV in the CNS. Recent evidence using high throughput sequencing, *in situ* hybridization and immunocytochemical studies suggest that VMAT₁ is also present in the CNS, where it is concentrated to the SN and has been implicated in the etiology of schizophrenia [70–75].

VMAT Regulation

Our current understanding of VMAT₂ regulation stems from the extent to which neurotoxic agents affect vesicular transport. VMAT₂ is inhibited by psychotherapeutic drugs, stimulants and metabolites such as, reserpine (RES), tetrabenazine (TBZ), methamphetamine (METH), amphetamine (AMPH), and 1-methyl-4-phenyl-1,2,3,6-tetrahydropyridine, and MPTP a prodrug of the neurotoxin MPP⁺ [63,64,76,77]. AMPH and METH are transported inhibitors of VMAT₂ while RES and TBZ are non-transported inhibitors. Increased cytoplasmic METH and AMPH are transported by VMAT₂ and promote the extrusion of vesicular DA into the cytoplasm thereby increasing cytosolic DA [63]. A consequence of increased cytosolic DA is the formation of toxic metabolites that are associated loss of DA neurons in diseases like Parkinson's, and thus, it is of interest to elucidate the intracellular mechanisms by which VMAT₂ transport is regulated.

We hypothesized that under normal physiological conditions, DA neurons that use VMAT₂ for vesicular filling maybe self-regulated and that spillover of DA may provide a mechanism for the intracellular regulation of VMAT₂. In DA neurons spillover from vesicular filling and increased cytosolic DA could initiate a signaling cascade that regulates VMAT₂. TAAR1, which is activated by DA and leads to elevation in cyclic AMP (cAMP) could modulate VMAT₂ activity. In 1995, Nakanishi and colleagues demonstrated that treatment of digitonin-permeabilized PC12 cells with dibutyl cyclic AMP (dbcAMP), reduced VMAT₂-mediated uptake [78], while PKA inhibitors increased VMAT₂ uptake [78]. However, the receptors, intracellular signaling proteins and precise mechanism responsible for endogenous cAMP-dependent regulation of VMAT₂ has not been addressed. It is also unclear whether a cAMP-dependent mechanism for regulation of VMAT₂ occurs in neurons.

VMAT₂ and TAAR1

Localization of TAAR1 in monoaminergic brain regions including the nigrostriatal and mesolimbic dopaminergic pathways that use the vesicular transporter, VMAT₂, suggests that TAAR1 might be well positioned to regulate monoaminergic neurotransmission [7,10,13]. Given TAAR1's intracellular location and its ability to increase cAMP, it is conceivable that TAAR1 could serve as a sensor of cytosolic monoamines and their metabolites to regulate VMAT₂ activity. The present study seeks to examine whether TAAR1-mediated activation of G α _s-AC-cAMP-PKA signaling can regulate VMAT₂ function using three model cell lines that express VMAT₂: SK-N-SH cells that express both VMAT₂ and TAAR1, an SK-N-SH cell line in which CRISPR-

Cas9 technology was used to knockout the endogenous TAAR1 protein gene and cultured murine midbrain DA neurons.

CHAPTER TWO: SPECIFIC AIMS

As previously described, VMAT₂ has been shown to be intracellularly regulated by activators of PKA like cAMP. However, the mechanism and upstream signaling molecules responsible for cAMP-dependent regulation of VMAT₂ has not been described. The ability for TAAR1 to elevate cAMP, as well as, its co-expression with VMAT₂ in DA neurons suggests that TAAR1-signaling may regulate VMAT₂ function. Towards investigating this we address the following specific aims:

- 1) To determine whether VMAT₂ is regulated by PKA agonists like cAMP in SK-N-SH cells.
- 2) To examine whether TAAR1 is essential for VMAT₂ regulation by comparing the effects of TAAR1 activation on VMAT₂ activity in wild type SK-N-SH cells to those observed in an SK-N-SH line in which the TAAR1 gene is disrupted.

The neuroprotective and vesicular filling roles of VMAT₂ in the brain depend on its function in regulating cytoplasmic and vesicular catecholamine content, but the physiological intracellular mechanisms that work to regulate VMAT₂ remain unclear. Therefore, knowledge from this study will provide new insight on intracellular regulation of VMAT₂, towards understanding the consequence of VMAT₂ dysregulation in disease.

MATERIALS & METHODS

Materials

Antibodies: Tyrosine hydroxylase (TH) polyclonal antibodies were acquired from AVES labs (anti-Chicken, Cat #TYH). Rabbit anti-VMAT₂ antibody (cat# ab191121) was purchased from Abcam. DAT antibody was generated in house as previously described [19,21]. Secondary antibodies donkey anti-mouse HRP and donkey anti-rabbit HRP were acquired from Jackson Immuno Research Laboratories Inc (cat# 715-035-150) and Pierce (cat# 31458), respectively.

Tritiated Neurotransmitters: [³H] Dopamine (3,4[7-³H] dihydroxyphenylethylamine) and [³H] 5-hydroxytryptamine (5-HT, serotonin) were both purchased from PerkinElmer Life and Analytical Sciences (Waltham, MA).

Drugs and Toxins: Desipramine (cat# D3900), Mg²⁺ATP (cat #A9187), reserpine (cat# 83580) and dibutyryl cAMP (cat# D026) were acquired from Sigma Aldrich Chemical Co (St. Louis, MO). Unlabeled serotonin (cat# H953), and DA hydrochloride (cat# H8502) were also acquired from Sigma Aldrich. GBR12909 dihydrochloride (cat# 0421), *p*-trifluoromethoxyphenylhydrazone (FCCP, cat# 0453) and cAMPs-Rp, triethylammonium salt (cat# 1337), were purchased from Tocris (Ellisville, MO). PKA specific inhibitor KT5720 was acquired from A.G. Scientific (cat# K-1010). Reagents for SDS-PAGE, Bicinchoninic Bradford Protein Assay, Dulbecco's Modified Eagle's Medium (DMEM), fetal bovine serum (FBS) and all other culture media components

were purchased from Invitrogen/Life Technologies. cOmplete™ Mini EDTA-free Protease Inhibitor Cocktail, (cat# 11836170001) was acquired from Roche Diagnostics (IN, USA).

Methods:

Primary Neurons: Primary DA neurons were prepared from midbrain tissue dissected from embryonic day15 (E15) Swiss Webster mice as previously described [21]. All procedures and experiments with mice were performed in accordance with the NIH Guide for the Care and Use of Laboratory Animals and with the approval of the Institutional Animal Care and the Animal Care and Use Committee of the NIH. Midbrain tissue was subsequently triturated and plated at a density of 2 midbrains per 6×25 mm or 12×12 mm on poly-D-lysine coated glass coverslips (Warner Instruments). Cultures were maintained in DMEM supplemented with 5 % horse serum and 5 % calf serum for 14 to 28 days before being used for each experiment.

Cell Culture: SK-N-SH cells were obtained from ATCC (Rockville, MD, U.S.A.) and maintained in Dulbecco's Modified Eagles Medium with 5 % FBS and 0.1 % Penicillin/Streptomycin (P/S) at 37 °C in 5 % CO₂. Cells were grown in 75 cm² flasks and later transferred to 96 well plates or plated on 12 mm poly-D-lysine (10 µg/mL) coated glass coverslips and allowed to proliferate to reach confluence prior to initiating experiments. All cell culture assays were performed on cultures from at least three different plating procedures. Where possible, experiments were performed blindly.

Knock Out Cell Line: The TAAR1 KO cell line (Appendix 2A) generated in Chapter I was all used in this study. See materials and methods in Chapter I for details.

Vesicular Monoamine Uptake: SK-N-SH cells were plated in 96 well plates and primary DA neurons were plated on 12 mm glass coverslips. The cells were permeabilized with digitonin (10 μ M, 10–15 minutes) in DMEM and then equilibrated in uptake PBSK+ buffer containing: 2.7 mM NaCl, 137 mM KCL, 10 mM Na₂HPO₄, 1.8 mM KH₂PO₄, 2.5 mM Mg²⁺-ATP, pH 7.5 and GBR12909 (10 μ M). The cells were incubated with 10 μ M reserpine for ten minutes, unless otherwise noted, and uptake assays were initiated by the addition of 20 μ M unlabeled DA and 50–60 nM [³H]-DA in uptake buffer for 5 minutes at room temperature (RT). Uptake was terminated by two rapid washes with 50 μ L PBS-CM (PBS with 100 μ M CaCl₂ and 1 mM MgCl₂). Cells were then solubilized in 50 μ L of Bio-safe II scintillation fluid (RPI, Research Product International) and radioactivity was measured using a Microplate Liquid Scintillation Counter (model 2450 Perkin Elmer, MicroBeta2) or a LS 6500 Multipurpose Liquid Scintillation Counter (Beckman Coulter). In parallel, non-specific uptake of [³H]-DA or [³H] 5-HT was determined in the presence of GBR12909 (10 μ M) and desipramine (100 nM) and subtracted from total uptake to calculate specific VMAT₂-mediated uptake. Data analysis was performed using Prism 7.0 (GraphPad Software Inc., San Diego, CA). Results are given as means \pm SEM from more than three experiments performed in hexads on cells from different plating procedures.

Immunohistochemistry: Cells were fixed in 4 % paraformaldehyde at RT for 15 minutes. After three washes with phosphate–buffered saline (PBS), cells were permeabilized with 0.20 % Triton X–100 for 5 minutes and blocked with 5 % normal goat serum (NGS) for 2 h at room temperature before incubation with primary antibodies diluted in 5 % NGS overnight at 4 °C on a shaker. Primary antibodies were removed with three PBS washes and secondary antibodies applied in 5 % NGS at RT for 2 h. Secondary antibodies were washed off and coverslips were mounted in Fluoromount™ Aqueous Mounting Medium (cat# F4680; Sigma Aldrich) for subsequent confocal microscopy.

RESULTS

VMAT₂–mediated, reserpine sensitive uptake in midbrain DA neurons

Midbrain (MB) DA neurons express the twelve–transmembrane vesicular monoamine transporter 2 (VMAT₂), which regulates cytoplasmic catecholamine levels. DA synthesized by the cell and extracellular DA that is transported into the cytoplasm by the DAT is concentrated into vesicles by VMAT₂ in a proton and ATP–dependent manner. Preliminary data from the Amara laboratory demonstrated that both DAT and VMAT₂ are expressed in MB DA neurons in culture (Figure 2.1A). To assess VMAT₂ specific function, we exploited the VMAT₂ inhibitory ligand reserpine [79,80]. Digitonin–permeabilized primary neurons were pre–incubated with a buffer mimicking the intracellular environment, the DAT inhibitor GBR12909 and ATP (required for VMAT₂ uptake) in the presence or absence of reserpine. GBR12909 was added to ensure that we were measuring VMAT₂–specific uptake and not DAT–mediated uptake in incompletely permeabilized cells. Following preincubation with reserpine, 20 μ M of unlabeled DA and 50 nM [³H]–DA was added to the neurons for 5 minutes at RT. Reserpine potently reduced VMAT₂ uptake greater than 70 % of control ($p < 0.0001$) and required the presence of ATP (Figure 2.1B). In addition, disruption of the pH gradient and increased proton (H⁺)–permeability of the synaptic vesicle lipid bilayer by protein–independent uncoupler, carbonyl cyanide *p*–trifluoromethoxyphenylhydrazone (FCCP) also blocked reserpine–sensitive VMAT₂–mediated DA uptake (Figure 2.1B).

PKA Stimulation regulates VMAT₂ sensitive DA uptake in midbrain neurons

Endogenous DA spillover from maximal vesicular filling might be a physiological self-regulator of VMAT₂ transport. To date, intracellular regulation of VMAT₂ has not been fully described. We hypothesized that protein kinase A, PKA, may serve as an intracellular regulator of VMAT₂ in DA neurons. To test this hypothesis, we conducted VMAT₂-mediated uptake assays on MB DA cultures in the presence of commercially available PKA agonists and antagonists. Treatment of MB DA neurons with dibutyryl cAMP, a cell permeable analogue of cAMP, to activate PKA resulted in decreased reserpine-sensitive [³H]-DA VMAT₂ uptake (52.55 ± 9.86 %; $n = 12$) *in vitro* compared to control (Figure 2.1C). Similarly, activation of adenylyl cyclase with forskolin generated a dramatic decrease in VMAT₂ uptake, 53.7 ± 9.34 % ($n = 14$) of vehicle control. Conversely, treatment of MB DA neurons with a selective allosteric PKA inhibitor, KT 5720, and RpcAMPs an inhibitor of cAMP resulted in a significant increase in VMAT₂-mediated uptake *in vitro* ($p < 0.01$ and $p < 0.001$ respectively; Figure 2.1C). These data indicate that PKA negatively regulates VMAT₂ activity in DA neurons and that upstream signaling protein(s) and receptor(s) may be important for initiating this pathway. We hypothesized that activation of a GPCR by DA that stimulates cAMP elevation like TAAR1, or the dopamine receptor 1 (DRD1) could act as sensors to regulate cytoplasmic DA and synaptic vesicle filling by VMAT₂ (Figure 2.1D). Furthermore, activation of TAAR1-G α _s-AC-cAMP-PKA signaling by high cytoplasmic DA may induce downregulation of VMAT₂-mediated uptake (Figure 2.1D).

Blocking G α s increases reserpine-sensitive VMAT₂-mediated uptake

AC may be activated by several stimuli including the G α stimulatory G-protein (G α _s) resulting in the activation of PKA. DRD1 and TAAR1 are two GPCRs that are integral and requisite for maintaining function of DA neurons [7,81]. Activation of both receptors leads to activation of G α _s G-proteins and elevation of intracellular cAMP. To assess whether cAMP-dependent modulation of VMAT₂ in MB DA neurons is mediated by a GPCR we used a variety of α -subunit interfering peptides. The G α specific inhibitors (Figure 2.2A) were generated by the fusion of the cell permeable peptide sequence of HIV transactivator (TAT, 47–57) protein (GRKKRRQRRRPQ) and alpha interfering mini-gene sequences [82,83]. These interfering peptides block specific alpha subunits of heterotrimeric G-protein complexes preventing them from being activated by GPCRs and guanine nucleotide exchange factors (Figure 2.2A). Treatment of primary cultures with G α ₁₃ (TAT–13) and G α _s (TAT–R Control) interfering peptides did not affect reserpine-sensitive VMAT₂-mediated uptake (Figure 2.2A). However, inhibition of G α _s by TAT–S resulted in increased reserpine-sensitive VMAT₂-mediated ³H-DA uptake. TAT–S increased vesicle contents of DA by 210.8 ± 38.3 %; n = 6 (*p* value ≤ 0.0130) over control (Figure 2.2A).

The observed increase in VMAT₂ uptake in response to the inhibition of G α _s suggests that the stimulation of a GPCR that signals through the G α _s pathway is responsible for cAMP-mediated VMAT₂ regulation. We next examined the potential of DRD1 receptors to modulate VMAT₂ activity. Blocking DRD1 receptors with D1/D2 antagonists did not affect TAT–S induced reserpine-sensitive VMAT₂-mediated uptake

(Figure 2.2B). Since TAAR1 has also been shown to activate the $G_{\alpha s}$ pathway [1,2], we hypothesized that this GPCR may serve as an intracellular DA sensor. The presence of TAAR1 and VMAT₂ in SK–N–SH cells as well as the robust DA uptake capacity of these cells, compelled us to evaluate whether inhibition of VMAT₂ uptake by cAMP/PKA could be observed in SK–N–SH TAAR1 knockout cell lines.

Time course of the effect of reserpine on VMAT₂ [³H]–DA uptake

The time course of the effect of reserpine (10 μ M) on [³H]–DA uptake in SK–N–SH cells was determined. SK–N–SH cells were pre–incubated with reserpine followed by the addition of [³H]–DA. VMAT₂–mediated uptake was significantly reduced (53.33 ± 6.68 %; n = 9) after 10 min of pre–incubation (Figure 2.3). Note that reserpine was also present during the uptake assay. Exposure of SK–N–SH cells to reserpine for 30 minutes decreased [³H]–DA uptake to 37.59 ± 8.89 % (n = 10) of control (Figure 2.3), which was similar to the VMAT₂ uptake observed in the absence of digitonin permeabilization (38.98 ± 3.23 % (n = 10) of control) indicating that reserpine sensitive, VMAT₂–mediated uptake can successfully be measured in these cells using this method.

Characterization of SK–N–SH TAAR1 knockout cell line

SK–N–SH cells express TAAR1 and VMAT₂ and form functional neurotransmitter vesicles reminiscent of the small synaptic vesicles (SSV) found in neurons (Figure 2.4). CRISPR–Cas9 technology was used to generate the TAAR1 knockout SK–N–SH cell line (See Appendix 2A). TAAR1 deletion did not affect the cellular morphology of the SK–N–SH cells (Figure 2. 4A). Both wild–type SK–N–SH

and the TAAR1 knockout cell lines express the VMAT₂ protein as evidenced by western blot analysis and immunohistochemistry, respectively (Figures 2.4B, C).

cAMP-dependent regulation of VMAT₂ is not TAAR1 dependent

To determine whether the cAMP-induced reduction in VMAT₂ function observed in MB neurons was dependent on the TAAR1-G α_s -AC-cAMP-PKA signaling pathway, we compared the effect of PKA on VMAT₂ uptake in TAAR1 KO cell lines. There was no observed difference in uptake between wildtype SK-N-SH cells and TAAR1 KO cells treated with dbcAMP, forskolin, Rp-cAMPs or KT5720 drugs (Figure 2.5A). VMAT₂-mediated serotonin (5-HT) uptake which is a more effective substrate for VMAT₂ (DA, K_I = 25 \pm 7 μ M vs. 5-HT, K_I = 19 \pm 4 μ M) [63], and less effective agonist of TAAR1 [2] also resulted in no change in sensitivity to cAMP modulation (Figure 2.5B). These data indicate that in SK-N-SH cells cAMP downregulation of VMAT₂ activity is not mediated by TAAR1.

DISCUSSION

The pathologies of addiction, schizophrenia and Parkinson's disease all indicate dysregulation of catecholamine filling, storage and release by synaptic vesicles in the dopaminergic pathways of the brain [63,84]. As VMAT₂ is a key regulator of catecholamine storage and release in the DA neuron, it is of interest that we understand the physiological mechanisms that regulate VMAT₂. A mechanism that regulates filling of neuronal synaptic vesicles by VMAT₂ and their transmitter content has not clearly been identified. Over–twenty years ago, a Japanese laboratory first demonstrated that the secondary messenger cAMP regulates the function of VMAT₂ transport in endocrine derived pheochromocytoma (PC 12) cells [78,85]. These data implicated cAMP as an intracellular regulator of vesicular transport and filling by VMAT₂. However, the intracellular protein effectors affecting cAMP modulation of VMAT₂ activity have not been explored. Furthermore, it is unclear whether this mechanism of cAMP–dependent VMAT₂ regulation is present in neuronal vesicles and cells. We report here that in two cell lines and primary cultures that cAMP can serve as an intracellular regulator of VMAT₂ activity. Further, we have evaluated the role of the D1DR1 and TAAR1 in this signaling pathway. Our data supports that G α _s coupled GPCRs may be involved in cAMP–dependent regulation of VMAT₂ since inhibition of G α _s G–proteins resulted in a marked increase in VMAT₂ transport as compared with control groups. As both GPCR's are activated by DA which leads to increases in cAMP, it is possible that under normal conditions spillover of DA above normal vesicular filling capacity may trigger a VMAT₂ regulation cascade.

Nakanishi and colleagues evaluated the effect of cAMP on vesicular monoamine transport in large dense core vesicles (LDCV) present in PC12 cells in the PNS. However, we chose to study SK-N-SH cells which contain small synaptic vesicles (SSV), and better model the synaptic vesicles responsible for neurotransmitter storage in neurons of the CNS [62,69]. Additionally, MB DA neuronal cultures also express VMAT₂ in SSV. Therefore, both SK-N-SH and MB DA neuronal cultures provide a better model system to further explore cAMP-dependent regulation of VMAT₂ in the brain. We sought to ask the following questions: [1] Can cAMP also regulate VMAT₂ uptake in MB DA neurons and SK-N-SH cells? [2] Does blocking the α -subunit of G α _s heterotrimeric G-proteins modulate vesicular monoamine transport? and [3] Which G α _s coupled GPCR can serve as an intracellular sensor of monoamines and subsequent regulation of VMAT₂?

Herein, we developed a system for measuring VMAT₂-mediated, reserpine-sensitive DA uptake in primary neurons and SK-N-SH cells. In these cell systems VMAT₂ activity is sensitive to treatment with reserpine and cAMP in the presence of ATP. Both dbcAMP and forskolin, are similarly effective at downregulating VMAT₂ activity. In MB DA neurons and SK-N-SH cells cAMP-dependent reduction in VMAT₂ uptake is consistent with previous reports in PC12 cells [78]. Further, the protein kinase inhibitor, KT 5720, and the cAMP inhibitor, Rp cAMPs, resulted in increased vesicular DA uptake suggesting that cAMP-sensitive protein phosphorylation via the PKA pathway may regulate VMAT₂ uptake.

PKA activation can be mediated via activation of the $G\alpha_s$ -AC-cAMP pathway. Using a variety of α -subunit specific inhibitors we showed that cAMP-dependent modulation of VMAT₂ in MB DA neurons was mediated by $G\alpha_s$ signaling. Inhibition of DRD1 using DRD1/2 antagonists to block DRD1- $G\alpha_s$ -AC-cAMP signaling did not affect TAT-S induced increase in VMAT₂ sensitive transport of DA in MB DA neurons *in vitro*. Activation of $G\alpha_s$ coupled TAAR1 receptors by DA increases cAMP. TAAR1 knockout SK-N-SH cells were used to implicate TAAR1 in cAMP-dependent regulation of VMAT₂. Treatment of both cell lines with cAMP analogues lead to downregulation of vesicular monoamine transport while treatment with kinase inhibitors led to increased vesicular uptake suggesting that TAAR1 does not mediate cAMP-dependent regulation of VMAT₂. Serotonin, a higher affinity substrate for VMAT₂ and less potent agonist of TAAR1 resulted in no observed difference uptake in both cells lines.

The regulation of VMAT₂ by G-proteins is a complex phenomenon that may change dependent on cellular requirements and cell type. Different cell types may have a different array of intracellular signaling machinery to regulate VMAT₂ function. For example, Anherter and colleagues reported that $G\alpha_{o2}$ and $G\alpha_q$ activity downregulate VMAT_{1&2}-mediated transport in neuroendocrine cells and VMAT₂ in neurons [86-88]. $G\alpha_{o2}$ also regulates the vesicular glutamate transporters by modulating its chloride dependence [89] suggesting a mechanism by which this regulation could occur.

cAMP-dependent protein phosphorylation of tyrosine hydroxylase (TH), the rate-limiting enzyme in catecholamine biogenesis, enhances TH activity and monoamine synthesis [90,91]. One could speculate that the observed cAMP-dependent reduction in

VMAT₂ DA uptake was caused by increased intracellular DA synthesis due to increased TH activity. In effect, increased TH activity could increase endogenous DA concentrations, which may compete with [³H]-DA during uptake. The uptake assay contained 20 μM of unlabeled DA which is 500-fold greater than the 60 nM of radiolabeled DA used for uptake, indicating that TH upregulation and dilution of the radiolabel is unlikely to account for the reduced VMAT₂ DA uptake. cAMP treatment resulted in a similar reduction of VMAT₂ serotonin uptake (Figure 2.6B), which is independent of TH activity and has a higher affinity for VMAT₂ than DA (DA, K_I = 25 ± 7 μM; 5-HT, K_I = 19 ± 4 μM) [63,92,93]. However, to completely rule out the effect of TH on VMAT₂ activity, in the presence of cAMP more experiments will be conducted. Further, we will look at the effects of cAMP in the presence of a TH inhibitor like alpha methyl-p-tyrosine.

In summary, we have shown that cAMP/PKA reduces reserpine-sensitive VMAT₂ mediated DA uptake in MB DA neurons and SK-N-SH cells. Further, inhibition of endogenous G_αs signaling abolished reserpine-sensitive VMAT₂ DA uptake in MB neurons *in vitro*. We explored whether G_αs coupled DRD1 or TAAR1 were responsible. Inhibition of DRD1 by D1/D2 antagonist and G_αs inhibitory peptides did not attenuate reserpine-sensitive VMAT₂ activity in MB DA neurons. In SK-N-SH cells lacking TAAR1 no difference in VMAT₂ uptake is observed when treated with cAMP or PKA antagonists. These data indicate that neither DRD1 nor TAAR1 mediates G_αs or cAMP-dependent regulation of VMAT₂ activity.

Our current understanding of VMAT₂ focuses on its regulation by physiological stressors and drugs [84]. For example, in the brain this is especially the case in the dopaminergic neurons where drugs of abuse alter dopamine availability in the synapse and cytoplasm. Some of these changes in cytoplasmic and synaptic dopamine are in part regulated by VMAT₂. Therefore, understanding the physiological mechanisms governing VMAT₂ DA transport and storage is of interest. Our findings herein, provide evidence for cAMP-dependent regulation of VMAT₂ in DA neurons and suggests that under normal physiological circumstances elevated cytoplasmic DA and/or G α _s signaling may be responsible for initiating this signaling cascade. In effect, our data provides a basis intracellular regulation of VMAT₂. Further exploration of this work could expand our understanding of VMAT₂ regulation and may provide insight into how VMAT₂ dysregulation manifests in disorders like drug addiction schizophrenia, and Parkinson's.

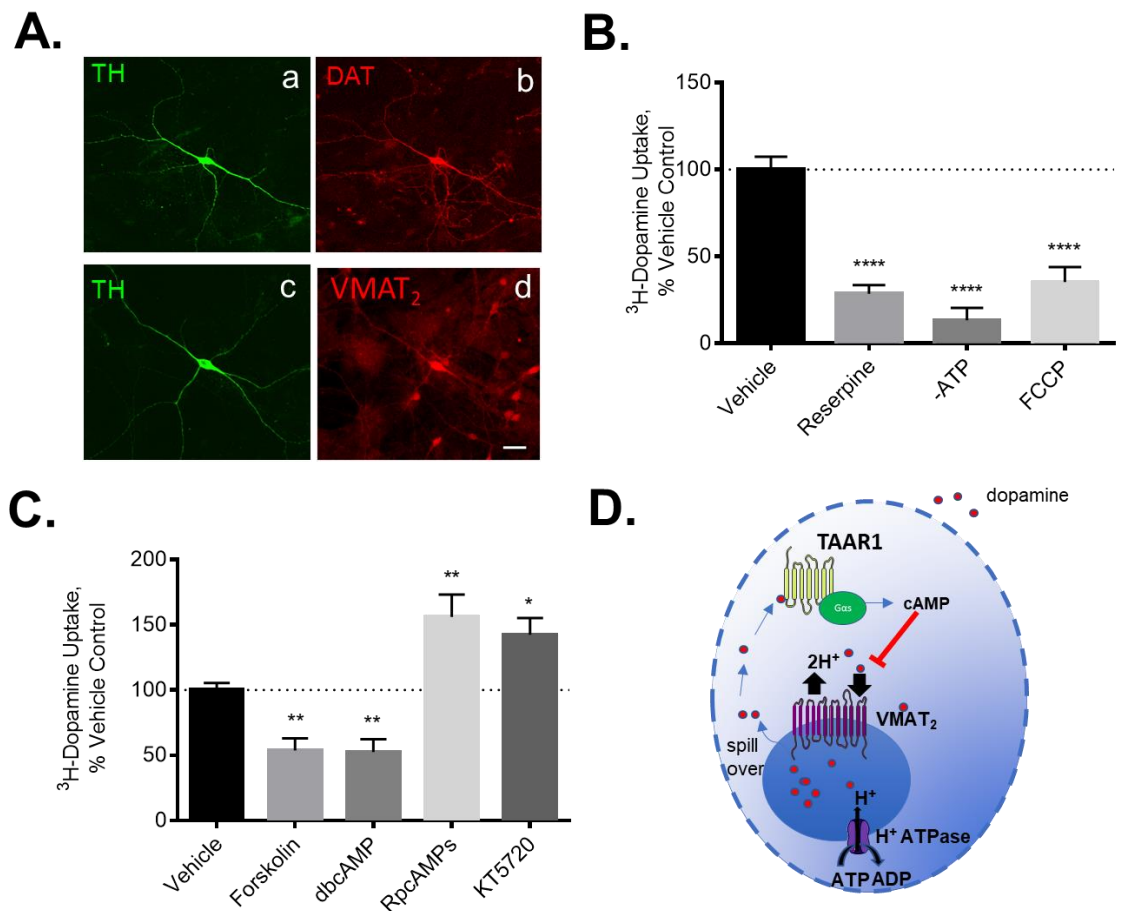


Figure 2.1: cAMP-dependent downregulation of VMAT₂ activity in MB DA neurons. (A) VMAT₂ expression in MB Dopamine neurons is confirmed by immunolabeling. Midbrain DA neurons were grown in culture and stained for tyrosine hydroxylase (TH; green in a, and c), DAT (red, b) and VMAT₂ (red, d). Scale bar, 10 μm. (B) Reserpine-sensitive VMAT₂ uptake is dependent on ATP and pH. Digitonin permeabilized MB DA cultures were treated with reserpine, in the presence or absence of ATP and FCCP. Reserpine (10 μM) reduced VMAT₂-mediated uptake by 60%. In the absence of ATP, [³H]-DA uptake was reduced to 80% of controls. FCCP, which disrupts the pH gradient in SVs, also decreased [³H]-DA uptake further supporting that this is VMAT₂-mediated [³H]-DA uptake. (C) cAMP regulates vesicular VMAT₂ uptake. Midbrain DA neurons were treated with reserpine, dbcAMP, forskolin, RpcAMPs or KT 5720 prior to and during uptake measures. The data shown represent mean ± SEM of three or more experiments. (* p ≤ 0.05; ** p ≤ 0.01 and **** p ≤ 0.0001 by one-way ANOVA compared to vehicle control). (D) Schematic of proposed TAAR1 mediated, cAMP-dependent regulation of VMAT₂. Vesicular filling above normal capacity could lead to DA spillover and subsequent activation of TAAR1 or DRD1 and elevation in cAMP which inhibit VMAT₂ transport.

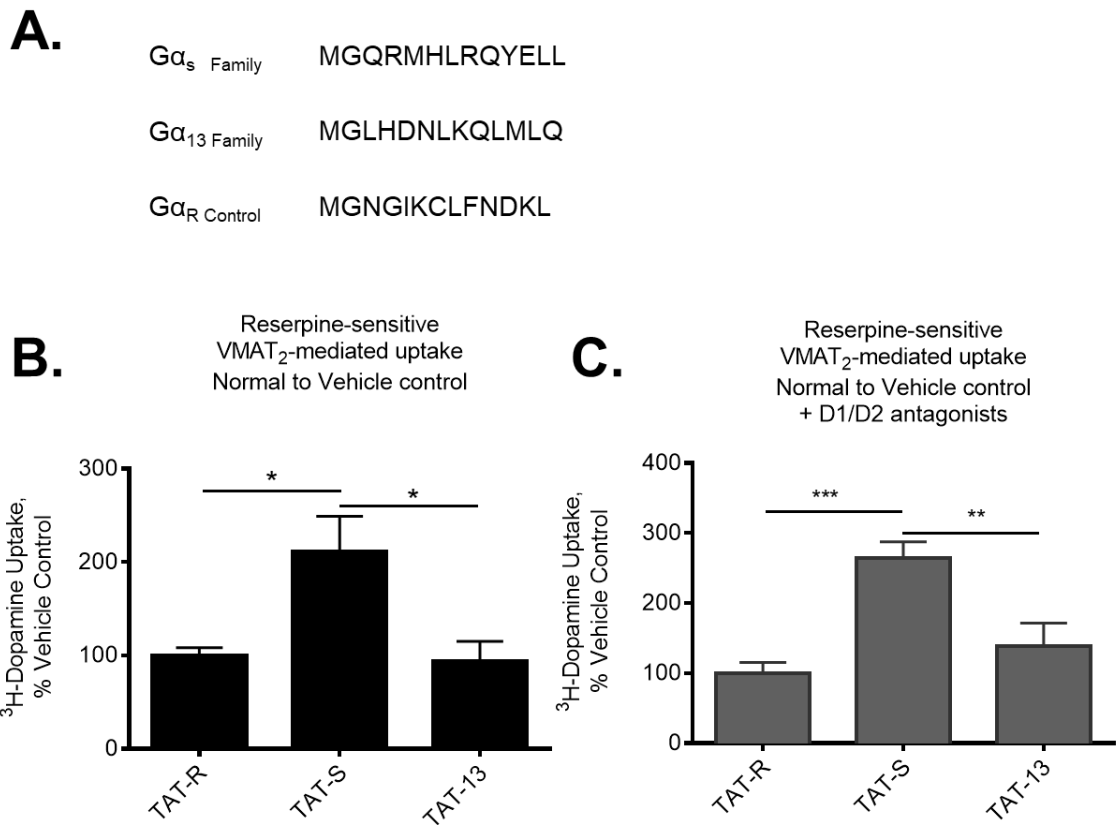


Figure 2.2: $G\alpha_s$ G-proteins downregulate reserpine-sensitive VMAT₂ uptake. (A) Amino acid alignment of specific $G\alpha$ inhibitory interfering peptides. Cell permeable interfering peptides were generated in the Amara lab by the fusion of these thirteen amino acid peptides to the TAT peptide [82,83]. The specific family of $G\alpha$ proteins which the peptide targets is also shown. $G\alpha_R$ was used as scrambled control. (B) Inhibition of $G\alpha_s$ increases VMAT₂ uptake. MB DA neurons were treated with cell permeable alpha-interfering peptides. In cells treated with TAT-S, VMAT₂ uptake was increased in comparison to that observed in the presence of the TAT-R and TAT-13 alpha interfering peptides. (C) Blocking DRD1 receptor does not abolish TAT-S induced increased in VMAT₂ uptake. Midbrain DA neurons were treated with D1/D2 receptor antagonists prior to treatment with cell permeable alpha-interfering peptides. In cells treated with TAT-S, blocking of DRD1 did not abolish TAT-S induced increased VMAT₂ uptake. TAT-R and TAT-13 control interfering peptides did not increase VMAT₂ activity. The data shown represents mean \pm SEM of three or more experiments. (* $p \leq 0.05$; ** $p \leq 0.01$ and *** $p \leq 0.001$ by one-way ANOVA).

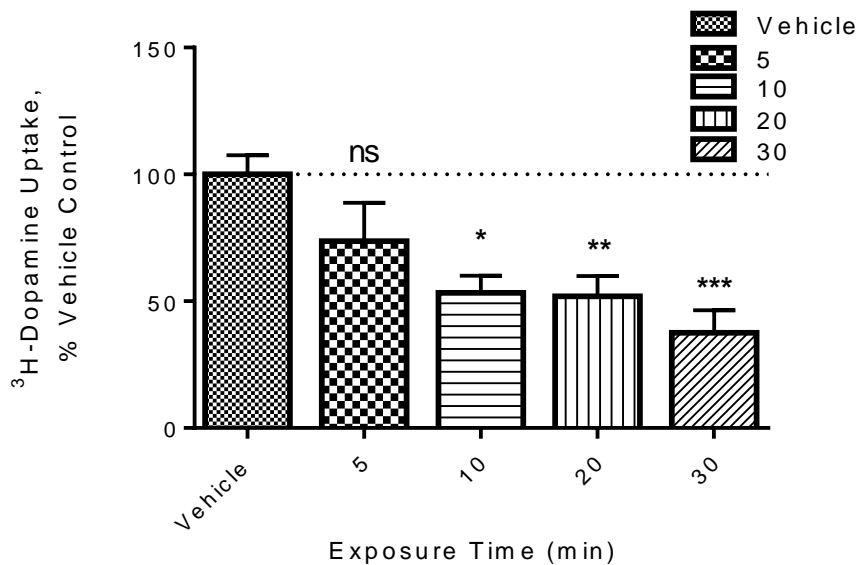


Figure 2.3: Time course of reserpine inhibition of VMAT₂ DA uptake in SK-N-SH cells. Digitonin-permeabilized cells were treated with reserpine for increasing amounts of time. After 10 minutes of exposure reserpine significantly reduced uptake by VMAT₂ to 50% of the vehicle control, indicating that this is a sufficient time-point for reserpine to diffuse into the permeabilized cells and inhibit VMAT₂-mediated DA uptake. All data points are represented as an average \pm SEM. Quantification was performed on four independent experiments. (* $p \leq 0.05$; ** $p \leq 0.01$ and *** $p \leq 0.001$ by one-way ANOVA; ns, statistically nonsignificant).

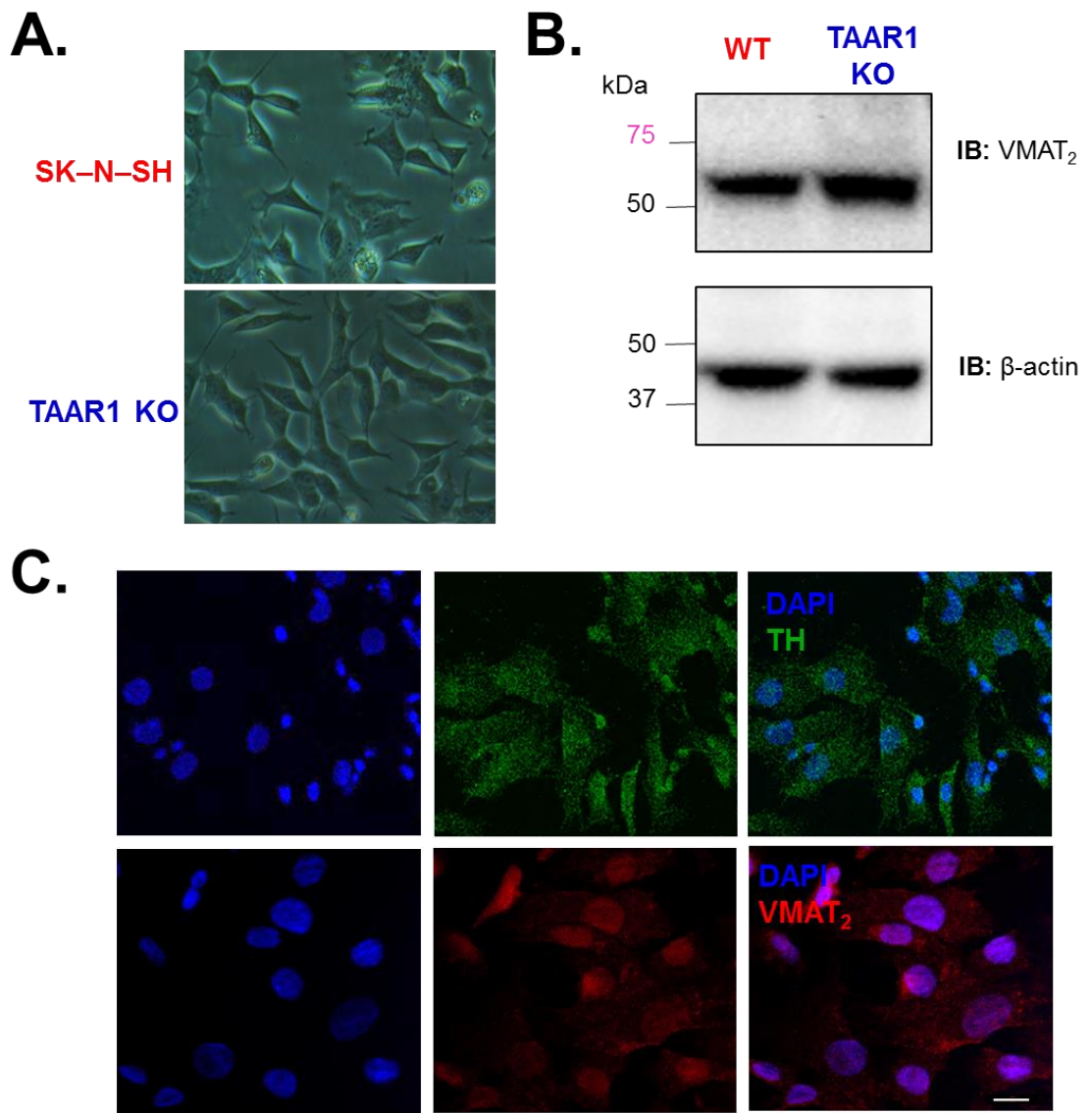


Figure 2.4: Deletion of TAAR1 does not change the morphology of the cells or the expression of VMAT₂. (A) Wildtype SK-N-SH cells and TAAR1 KO K-SN-SH cells have similar morphology as evidenced by DIC image. (B) Equal amounts of cell lysates from the wild-type (WT) and TAAR1 KO cells were analyzed by western blot for VMAT₂. Both cell types contain VMAT₂. β-actin further confirms similar protein concentrations in the two samples. (C) SK-N-SH cells express VMAT₂ and tyrosine hydroxylase (TH).

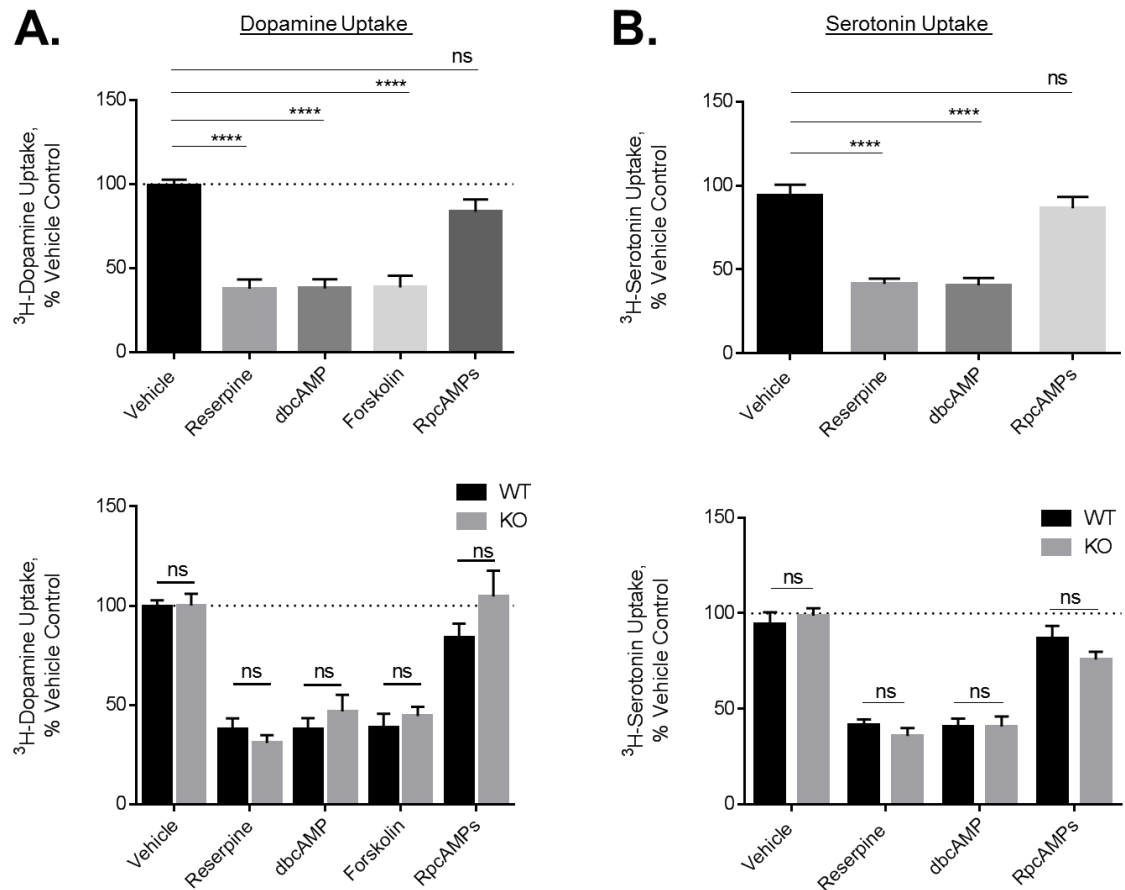
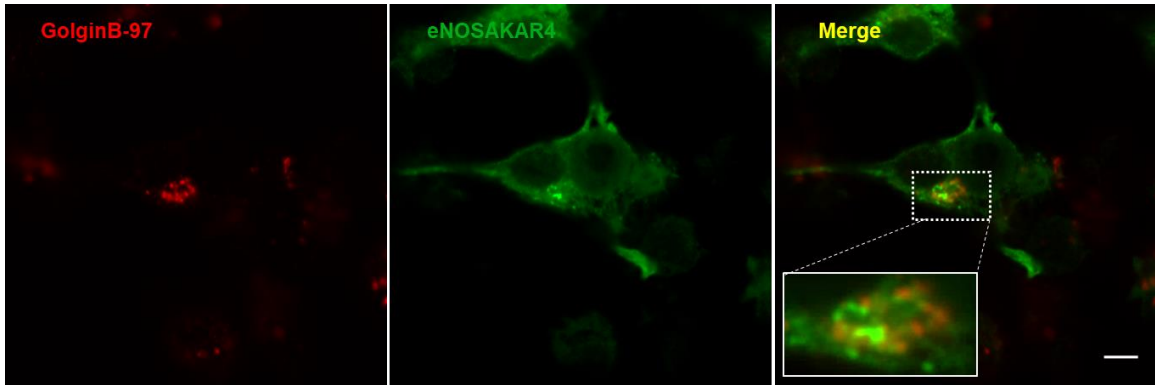


Figure 2.5: TAAR1 does not mediate cAMP-dependent VMAT₂ uptake in SK-N-SH cells. (A) *cAMP*-dependent VMAT₂ DA uptake. Digitonin-permeabilized WT and TAAR1 KO cells were treated with reserpine, dbcAMP, forskolin and RpcAMPs. Reserpine significantly reduced VMAT₂ DA uptake in both cell types. Forskolin and dbcAMP decreased VMAT₂ DA uptake while, inhibition of PKA by RpcAMPs increased VMAT₂ DA transport. In comparison WT, no difference in *cAMP*-dependent downregulation in VMAT₂ activity is present. (B) *cAMP*-dependent VMAT₂ serotonin (5-HT) uptake. Using 5-HT, we observed similar data. All data in bar graphs are presented as average \pm SEM from three or more independent experiments. (**** $p \leq 0.0001$ by two-way ANOVA; ns, statistically nonsignificant).

APPENDIX



Appendix 1A/ eNOSAKAR4 does not colocalize with trans-Golgi marker Golgin-97. Post transfection of HEK293 cells with eNOSAKAR4, the cells were stained with mouse monoclonal Golgin-97 antibody. Merged image show that GFP and Alexa 568 (Golgin-97) do not colocalize. In addition, the eNOSAKAR4 also shows noticeable cytoplasmic expression. Scale bar, 10 μ m.

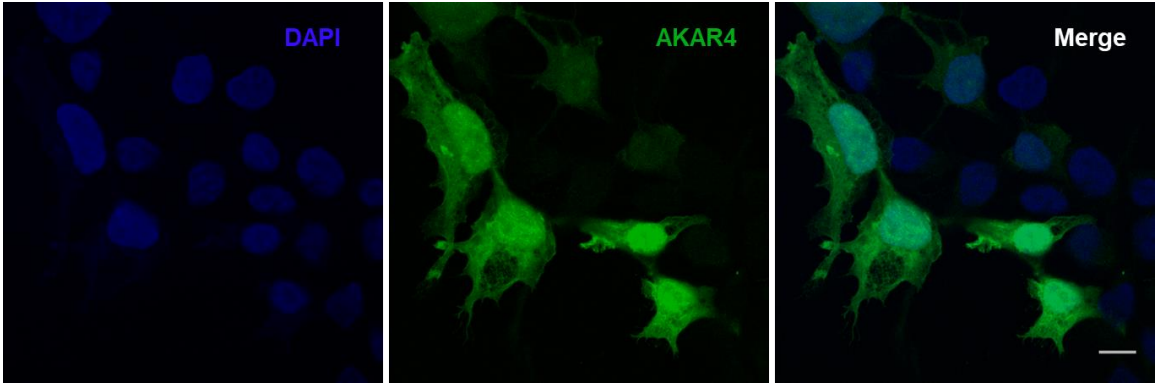
A.

Query	61	ATGATGCCCTTTTGCACAATATAATTAATATTTCTGTGTGAAAAACAACCTGGTCAAAT	120	TAAR1-KO
Sbjct	1	ATGATGCCCTTTTGCACAATATAATTAATATTTCTGTGTGAAAAACAACCTGGTCAAAT	60	TAAR1-WT
Query	121	GATGTCCGTGCTTCCCTGTA-AGTTTAATGGTGCTCATAATTCTGACCACACTCGTTGGC	179	
Sbjct	61	GATGTCCGTGCTTCCCTGTACAGTTAATGGTGCTCATAATTCTGACCACACTCGTTGGC	120	
Query	180	AATCTGATAGTTATTGTTTCTATATCACACTTCAAACAACCTTCATACCCAACAAATTGG	239	
Sbjct	121	AATCTGATAGTTATTGTTTCTATATCACACTTCAAACAACCTTCATACCCAACAAATTGG	180	

B.

M M P F C H N I I N I S C V K N N W S N D V R A S
L Stop

Appendix 2A| Development of CRISPR-Cas9 TAAR1 knockout SK-N-SH cell line. (A) Sequence alignment of the wildtype (WT) and knockout (KO) TAAR1 cDNA. The Cas9 endonuclease required protospacer adjacent motif (PAM) sequence indicated by the blue line caused the deletion of a cytosine nucleotide (red arrow), which resulted in a frameshift that generated a premature stop codon (red line). (B) Truncated TAAR1 KO Protein Sequence. The translation of the TAAR1 KO gene generates a truncated and twenty-six amino acid TAAR1 peptide. The TAAR1 KO Cells were provided by Dr. Jingshan Chen in the Amaralab. Scale bar, 10 μ m.



Appendix 3A| AKAR4 donor plasmid cellular distribution. The AKAR4 only plasmid shows whole cell distribution.

LIST OF JOURNAL ABBREVIATIONS

Adv Pharmacol	Advances in Pharmacology
Am J Physiol Cell Physiol	American Journal of Physiology Cell Physiology
Annu Rev Neurosci	Annual Review of Neuroscience
Biochem Biophys Res Commun	Biochemical and Biophysical Research Communications
Bioconjug Chem	Bioconjugate Chemistry
Brain Res Dev Brain Res	Brain Research Developmental Brain Research
Br J Pharmacol	British Journal of Pharmacology
Br J Pharmacol Chemother	British Journal of Pharmacology and Chemotherapy
Cell Biol	Cell Biology
Cell Rep	Cell Reports
Cell Signal	Cell Signalling
Dev Brain Res	Developmental Brain Research
Dev Cell	Developmental Cell
EMBO J	EMBO Journal
Eur J Cell Biol	European Journal of Cell Biology
Eur Thyroid J	European Thyroid Journal
FEBS Lett	FEBS Letters
Front Neurosci	Frontiers in Neuroscience
Front Pharmacol	Frontiers in Pharmacology
Genes Brain Behav	Genes, Brain and Behavior
JOP J Pancreas	JOP: Journal of the Pancreas

J Biol Chem	Journal of Biological Chemistry
J Cell Biol	Journal of Cell Biology
J Cell Sci	Journal of Cell Science
J Immunol	Journal of Immunology
J Mol Neurosci	Journal of Molecular Neuroscience
J Neurochem	Journal of Neurochemistry
J Neurosci	Journal of Neuroscience
J Pharmacol Exp Ther	Journal of Pharmacology and Experimental Therapeutics
Med Res Rev	Medicinal Research Reviews
Mol Biol Cell	Molecular Biology of the Cell
Mol Brain Res	Molecular Brain Research
Mol Pharmacol	Molecular Pharmacology
Neural Regen Res	Neural Regeneration Research
Neurochem Int	Neurochemistry International
Neuro Endocrinol Lett	Neuroendocrinology Letters
Pharmacol Res	Pharmacological Research
Pharmacol Rev	Pharmacological Reviews
PNAS	Proceedings of the National Academy of Sciences of the United States of America

Prog Neurobiol

Progress in Neurobiology

PLoS ONE

Public Library of Science (PLOS) One

Schizophr Res

Schizophrenia Research

Sci Signal

Science Signalling

REFERENCES

1. Borowsky B, Adham N, Jones KA, Raddatz R, Artymyshyn R, Ogozalek KL, Durkin MM, Lakhani PP, Bonini JA, Pathirana S, Boyle N, Pu X, Kouranova E, Lichtblau H, Ochoa FY, Branchek TA, Gerald C. Trace amines: Identification of a family of mammalian G protein-coupled receptors. *Proc Natl Acad Sci*. 2001 Jul 31;98(16):8966–71.
2. Bunzow JR, Sonders MS, Arttamangkul S, Harrison LM, Zhang G, Quigley DI, Darland T, Suchland KL, Pasumamula S, Kennedy JL, Olson SB, Magenis RE, Amara SG, Grandy DK. Amphetamine, 3,4-Methylenedioxymethamphetamine, Lysergic Acid Diethylamide, and Metabolites of the Catecholamine Neurotransmitters Are Agonists of a Rat Trace Amine Receptor. *Mol Pharmacol*. 2001 Dec 1;60(6):1181–8.
3. Berry MD. Mammalian central nervous system trace amines. Pharmacologic amphetamines, physiologic neuromodulators. *J Neurochem*. 2004 Jun 10;90(2):257–71.
4. Axelrod J, Saavedra JM. Octopamine. *Nature*. 1977 Feb 10;265(5594):501–4.
5. Burchett SA, Hicks TP. The mysterious trace amines: Protean neuromodulators of synaptic transmission in mammalian brain. *Prog Neurobiol*. 2006 Aug;79(5–6):223–46.
6. Blackwell B, Mabbitt L. Tyramine in cheese related to hypertensive crises after monoamine-oxidase inhibition. *Lancet*. 1965 May 1;285(7392):938–40.
7. Pei Y, Asif-Malik A, Canales JJ. Trace Amines and the Trace Amine-Associated Receptor 1: Pharmacology, Neurochemistry, and Clinical Implications. *Front Neurosci*. 2016 Apr 5;10(148):1–17.
8. Crout JR, Muskus AJ, Trendelenburg U, Hobbs RD. Effect of tyramine on isolated guinea-pig atria in relation to their noradrenaline stores. *Br J Pharmacol Chemother*. 1962 Jun 17;18(3):600–11.
9. Lindemann L, Meyer CA, Jeanneau K, Bradaia A, Ozmen L, Bluethmann H, Bettler B, Wettstein JG, Borroni E, Moreau J-L, Hoener MC. Trace Amine-Associated Receptor 1 Modulates Dopaminergic Activity. *J Pharmacol Exp Ther*. 2007 Dec 19;324(3):948–56.
10. Xie Z, Miller GM. Trace Amine-Associated Receptor 1 Is a Modulator of the Dopamine Transporter. *J Pharmacol Exp Ther*. 2007 Jan 10;321(1):128–36.

11. Miller GM. Primate Trace Amine Receptor 1 Modulation by the Dopamine Transporter. *J Pharmacol Exp Ther.* 2005 Jan 28;313(3):983–94.
12. Szumska J, Qatato M, Rehders M, Fuhrer D, Biebermann H, Grandy DK, Kohrle J, Brix K. Trace Amine-Associated Receptor 1 Localization at the Apical Plasma Membrane Domain of Fisher Rat Thyroid Epithelial Cells Is Confined to Cilia. *Eur Thyroid J.* 2015 Jun 10;4(1):30–41.
13. Xie Z, Miller GM. Trace amine-associated receptor 1 as a monoaminergic modulator in brain. *Biochem Pharmacol.* 2009 Nov;78(9):1095–104.
14. Revel FG, Moreau J-L, Gainetdinov RR, Bradaia A, Sotnikova TD, Mory R, Durkin S, Zbinden KG, Norcross R, Meyer CA, Metzler V, Chaboz S, Ozmen L, Trube G, Pouzet B, Bettler B, Caron MG, Wettstein JG, Hoener MC. TAAR1 activation modulates monoaminergic neurotransmission, preventing hyperdopaminergic and hypoglutamatergic activity. *Proc Natl Acad Sci USA.* 2011;108(20):8485–90.
15. Alvarsson A, Zhang X, Stan TL, Schintu N, Kadkhodaei B, Millan MJ, Perlmann T, Svenningsson P. Modulation by Trace Amine-Associated Receptor 1 of Experimental Parkinsonism, L-DOPA Responsivity, and Glutamatergic Neurotransmission. *J Neurosci.* 2015 Oct 14;35(41):14057–69.
16. Wolinsky TD, Swanson CJ, Smith KE, Zhong H, Borowsky B, Seeman P, Branchek T, Gerald CP. The Trace Amine 1 receptor knockout mouse: an animal model with relevance to schizophrenia. *Genes Brain Behav.* 2007 Oct;6(7):628–39.
17. Cotter R, Pei Y, Mus L, Harmeier A, Gainetdinov RR, Hoener MC, Canales JJ. The trace amine-associated receptor 1 modulates methamphetamine's neurochemical and behavioral effects. *Front Neurosci.* 2015 Feb 13;9(39):1–9.
18. Pei Y, Lee J, Leo D, Gainetdinov RR, Hoener MC, Canales JJ. Activation of the Trace Amine-Associated Receptor 1 Prevents Relapse to Cocaine Seeking. *Neuropsychopharmacology.* 2014 Sep;39(10):2299–308.
19. Wheeler DS, Underhill SM, Stolz DB, Murdoch GH, Thiels E, Romero G, Amara SG. Amphetamine activates Rho GTPase signaling to mediate dopamine transporter internalization and acute behavioral effects of amphetamine. *Proc Natl Acad Sci.* 2015 Dec 22;112(51):E7138-7147.
20. Sukhanov I, Caffino L, Efimova EV, Espinoza S, Sotnikova TD, Cervo L, Fumagalli F, Gainetdinov RR. Increased context-dependent conditioning to amphetamine in mice lacking TAAR1. *Pharmacol Res.* 2016 Jan;103:206–14.

21. Underhill SM, Wheeler DS, Li M, Watts SD, Ingram SL, Amara SG. Amphetamine Modulates Excitatory Neurotransmission through Endocytosis of the Glutamate Transporter EAAT3 in Dopamine Neurons. *Neuron*. 2014 Jul 16;83(2):404–16.
22. Li M-H, Underhill SM, Reed C, Phillips TJ, Amara SG, Ingram SL. Amphetamine and Methamphetamine Increase NMDAR-GluN2B Synaptic Currents in Midbrain Dopamine Neurons. *Neuropsychopharmacology*. 2017 Jun;42(7):1539–47.
23. Kenakin T, Miller LJ. Seven Transmembrane Receptors as Shapeshifting Proteins: The Impact of Allosteric Modulation and Functional Selectivity on New Drug Discovery. *Pharmacol Rev*. 2010 Jun 1;62(2):265–304.
24. Masuho I, Ostrovskaya O, Kramer GM, Jones CD, Xie K, Martemyanov KA. Distinct profiles of functional discrimination among G proteins determine the actions of G protein–coupled receptors. *Sci Signal*. 2015 Dec 1;8(405):ra123–ra123.
25. Xie Z, Vallender EJ, Yu N, Kirstein SL, Yang H, Bahn ME, Westmoreland SV, Miller GM. Cloning, expression, and functional analysis of rhesus monkey trace amine-associated receptor 6: Evidence for lack of monoaminergic association. *J Neurosci Res*. 2008 Nov 15;86(15):3435–46.
26. Aronin N, DiFiglia M. The Subcellular Localization of the G-Protein Gia in the Basal Ganglia Reveals Its Potential Role in Both Signal Transduction and Vesicle Trafficking. *J Neurosci*. 1992 Sep;12(9):3435–44.
27. Ahnert-Hilger G, Schafer T, Spicher K, Grund C, Schultz G, Wiedenmann B. Detection of G-protein heterotrimers on large dense core and small synaptic vesicles of neuroendocrine and neuronal cells. *Eur J Cell Biol*. 1994 Oct;65(1):26–8.
28. Wuttke MS, Buck J, Levin LR. Bicarbonate-Regulated Soluble Adenylyl Cyclase. *JOP J Pancreas*. 2001;2(4):154–8.
29. Dunn TA, Storm DR, Feller MB. Calcium-Dependent Increases in Protein Kinase-A Activity in Mouse Retinal Ganglion Cells Are Mediated by Multiple Adenylate Cyclases. Hendricks M, editor. *PLoS ONE*. 2009 Nov 17;4(11):e7877.
30. Martin BR, Lambert NA. Activated G Protein $G\alpha_s$ Samples Multiple Endomembrane Compartments. *J Biol Chem*. 2016 Sep 23;291(39):20295–302.
31. Geng W, Wang Z, Zhang J, Reed BY, Pak CYC, Moe OW. Cloning and characterization of the human soluble adenylyl cyclase. *Am J Physiol-Cell Physiol*. 2005 Jun;288(6):C1305–16.

32. Asirvatham AL, Galligan SG, Schillace RV, Davey MP, Vasta V, Beavo JA, Carr DW. A-Kinase Anchoring Proteins Interact with Phosphodiesterases in T Lymphocyte Cell Lines. *J Immunol*. 2004 Oct 15;173(8):4806–14.
33. Langeberg LK. A-kinase-anchoring proteins. *J Cell Sci*. 2005 Aug 1;118(15):3217–20.
34. Aittaleb M, Gao G, Evelyn CR, Neubig RR, Tesmer JJG. A conserved hydrophobic surface of the LARG pleckstrin homology domain is critical for RhoA activation in cells. *Cell Signal*. 2009 Nov;21(11):1569–78.
35. Aittaleb M, Boguth CA, Tesmer JJG. Structure and Function of Heterotrimeric G Protein-Regulated Rho Guanine Nucleotide Exchange Factors. *Mol Pharmacol*. 2010 Feb 1;77(2):111–25.
36. Patel M, Kawano T, Suzuki N, Hamakubo T, Karginov AV, Kozasa T. G 13/PDZ-RhoGEF/RhoA Signaling Is Essential for Gastrin-Releasing Peptide Receptor-Mediated Colon Cancer Cell Migration. *Mol Pharmacol*. 2014 Jul 24;86(3):252–62.
37. Hart MJ, Sharma S, elMasry N, Qiu R-G, McCabe P, Polakis P, Gideon B. Identification of a Novel Guanine Nucleotide Exchange Factor for the Rho GTPase. *J Biol Chem*. 1996 Oct 11;271(41):25452–8.
38. Suzuki N, Hajicek N, Kozasa T. Regulation and Physiological Functions of G12/13-Mediated Signaling Pathways. *Neurosignals*. 2009 Feb;17(1):55–70.
39. Siehler S. THEMED ISSUE: GPCR REVIEW Regulation of RhoGEF proteins by G12/13-coupled receptors. *Br J Pharmacol*. 2009 Feb;158(1):41–9.
40. Miyawaki A. Visualization of the Spatial and Temporal Dynamics of Intracellular Signaling. *Dev Cell*. 2003 Mar;4(3):295–305.
41. Allen MD, Zhang J. Subcellular dynamics of protein kinase A activity visualized by FRET-based reporters. *Biochem Biophys Res Commun*. 2006 Sep;348(2):716–21.
42. Depry C, Zhang J. Using FRET-Based Reporters to Visualize Subcellular Dynamics of Protein Kinase A Activity. Luttrell LM, Ferguson SSG, editors. *Signal Transduct Protoc*. 2011 Jan;7(1):52–8.
43. Komatsu N, Aoki K, Yamada M, Yukinaga H, Fujita Y, Kamioka Y, Matsuda M. Development of an optimized backbone of FRET biosensors for kinases and GTPases. *Mol Biol Cell*. 2011 Dec 1;22(23):4647–56.
44. Patel N, Gold MG. The genetically encoded tool set for investigating cAMP: more than the sum of its parts. *Front Pharmacol*. 2015 Aug 6;6:1–11.

45. Pertz O, Hodgson L, Klemke RL, Hahn KM. Spatiotemporal dynamics of RhoA activity in migrating cells. *Nature*. 2006 Apr 20;440:1069–72.
46. Ray M, Tang R, Jiang Z, Rotello VM. Quantitative Tracking of Protein Trafficking to the Nucleus Using Cytosolic Protein Delivery by Nanoparticle-Stabilized Nanocapsules. *Bioconjug Chem*. 2015 Jun 17;26(6):1004–7.
47. Sessa WC, Garcia-Cardenas G, Liu J, Keh A, Pollock JS, Bradley J, Thiru S, Braverman IM, Desai KM. The Golgi Association of Endothelial Nitric Oxide Synthase Is Necessary for the Efficient Synthesis of Nitric Oxide. *J Biol Chem*. 1995 Jul 28;270(30):17641–4.
48. Sangwung P, Greco TM, Wang Y, Ischiropoulos H, Sessa WC, Iwakiri Y. Proteomic Identification of S-Nitrosylated Golgi Proteins: New Insights into Endothelial Cell Regulation by eNOS-Derived NO. Gaetano C, editor. *PLoS ONE*. 2012 Feb 21;7(2):e31564.
49. Huang LJ, Wang L, Ma Y, Durick K, Perkins G, Deerinck TJ, Ellisman MH, Taylor SS. NH₂-Terminal Targeting Motifs Direct Dual Specificity A-Kinase-anchoring Protein 1 (D-AKAP1) to Either Mitochondria or Endoplasmic Reticulum. *J Cell Biol*. 1999 May 31;145(5):951–9.
50. Ma Y, Taylor SS. A Molecular Switch for Targeting between Endoplasmic Reticulum (ER) and Mitochondria: CONVERSION OF A MITOCHONDRIA-TARGETING ELEMENT INTO AN ER-TARGETING SIGNAL IN DAKAP1. *J Biol Chem*. 2008 Apr 25;283(17):11743–51.
51. Miyamoto T, Rho E, Sample V, Akano H, Magari M, Ueno T, Gorshkov K, Chen M, Tokumitsu H, Zhang J, Inoue T. Compartmentalized AMPK Signaling Illuminated by Genetically Encoded Molecular Sensors and Actuators. *Cell Rep*. 2015 Apr;11(4):657–70.
52. Markwardt ML, Kremers G-J, Kraft CA, Ray K, Cranfill PJC, Wilson KA, Day RN, Wachter RM, Davidson MW, Rizzo MA. An Improved Cerulean Fluorescent Protein with Enhanced Brightness and Reduced Reversible Photoswitching. Jones D, editor. *PLoS ONE*. 2011 Mar 29;6(3):e17896.
53. Waites CL, Mehta A, Tan PK, Thomas G, Edwards RH, Krantz DE. An Acidic Motif Retains Vesicular Monoamine Transporter 2 on Large Dense Core Vesicles. *J Cell Biol*. 2001 Mar 19;152(6):1159–68.
54. Grygoruk A, Fei H, Daniels RW, Miller BR, DiAntonio A, Krantz DE. A Tyrosine-based Motif Localizes a Drosophila Vesicular Transporter to Synaptic Vesicles *in Vivo*. *J Biol Chem*. 2010 Mar 5;285(10):6867–78.

55. Groemer TW, Thiel CS, Holt M, Riedel D, Hua Y, Hüve J, Wilhelm BG, Klingauf J. Amyloid Precursor Protein Is Trafficked and Secreted via Synaptic Vesicles. Okazawa H, editor. PLoS ONE. 2011 Apr 27;6(4):e18754.
56. Szumska J. Trace amine-associated receptor 1 is involved in various aspects of endocrine regulation [Internet] [PhD Thesis]. 2017. Available from: <http://urn-resolving.de/urn:nbn:de:gbv:579-opus-1007442>
57. Rutigliano G, Accorroni A, Zucchi R. The Case for TAAR1 as a Modulator of Central Nervous System Function. *Front Pharmacol*. 2018 Jan 10;8(897).
58. Barak LS, Salahpour A, Zhang X, Masri B, Sotnikova TD, Ramsey AJ, Violin JD, Lefkowitz RJ, Caron MG, Gainetdinov RR. Pharmacological Characterization of Membrane-Expressed Human Trace Amine-Associated Receptor 1 (TAAR1) by a Bioluminescence Resonance Energy Transfer cAMP Biosensor. *Mol Pharmacol*. 2008 Jun 3;74(3):585–94.
59. Hochman S. Metabolic recruitment of spinal locomotion: intracellular neuromodulation by trace amines and their receptors. *Neural Regen Res*. 2015;10(12):1940.
60. Mehta S, Aye-Han N-N, Ganesan A, Oldach L, Gorshkov K, Zhang J. Calmodulin-controlled spatial decoding of oscillatory Ca²⁺ signals by calcineurin. *Cell Biol*. 2014 Jul 23;3(e03765):1–22.
61. Amara SG, Kuhar MJ. Neurotransmitter Transporters: Recent Progress. *Annu Rev Neurosci*. 1993 Mar;16(1):73–93.
62. Park Y, Kim K-T. Short-term plasticity of small synaptic vesicle (SSV) and large dense-core vesicle (LDCV) exocytosis. *Cell Signal*. 2009 Oct;21(10):1465–70.
63. Wimalasena K. Vesicular monoamine transporters: Structure-function, pharmacology, and medicinal chemistry. *Med Res Rev*. 2011 Jul;31(4):483–519.
64. Liu Y. A cDNA that suppresses MPP⁺ toxicity encodes a vesicular amine transporter. *Cell*. 1992 Aug 21;70(4):539–51.
65. Liu L, Xu W, Harrington KA, Emson PC. The molecular cloning and expression of a human synaptic vesicle amine transporter that suppresses MPP⁺ toxicity. *Mol Brain Res*. 1994 Aug;25(1–2):90–6.
66. STAAL RGW, SONSALLA PK. Inhibition of Brain Vesicular Monoamine Transporter (VMAT2) Enhances 1-Methyl-4-phenylpyridinium Neurotoxicity In Vivo in Rat Striata. 2018;293:7.

67. Erickson JD, Schafer MK, Bonner TI, Eiden LE, Weihe E. Distinct pharmacological properties and distribution in neurons and endocrine cells of two isoforms of the human vesicular monoamine transporter. *Proc Natl Acad Sci*. 1996 May 14;93(10):5166–71.
68. Nirenberg MJ, Liu Y, Peter D, Edwards RH, Pickel VM. The vesicular monoamine transporter 2 is present in small synaptic vesicles and preferentially localizes to large dense core vesicles in rat solitary tract nuclei. *Proc Natl Acad Sci*. 1995 Sep 12;92(19):8773–7.
69. Mandela P, Chandley M, Xu Y-Y, Zhu M-Y, Ordway GA. Reserpine-induced reduction in norepinephrine transporter function requires catecholamine storage vesicles. *Neurochem Int*. 2010 May;56(6–7):760–7.
70. Hansson SR. Ontogeny of vesicular monoamine transporter mRNAs VMAT1 and VMAT2 II. Expression in neural crest derivatives and their target sites in the rat. *Brain Res Dev Brain Res*. 1998 Sep 10;110(1):159–74.
71. Bly M. Mutation in the vesicular monoamine gene, SLC18A1, associated with schizophrenia. *Schizophr Res*. 2005 Oct;78(2–3):337–8.
72. Multani PK, Hodge R, Estévez MA, Abel T, Kung H, Alter M, Brookshire B, Lucki I, Nall AH, Talbot K, Doyle GA, Lohoff FW. VMAT1 deletion causes neuronal loss in the hippocampus and neurocognitive deficits in spatial discrimination. *Neuroscience*. 2013 Mar 1;232:32–44.
73. Ibanez-Sandoval O, Tecuapetla F, Unal B, Shah F, Koos T, Tepper JM. Electrophysiological and Morphological Characteristics and Synaptic Connectivity of Tyrosine Hydroxylase-Expressing Neurons in Adult Mouse Striatum. *J Neurosci*. 2010 May 19;30(20):6999–7016.
74. Ashe KM, Chiu W-L, Khalifa AM, Nicolas AN, Brown BL, Martino RRD, Alexander CP, Waggener CT, Fischer-Stenger K, Stewart JK. Vesicular monoamine transporter-1 (VMAT-1) mRNA and immunoreactive proteins in mouse brain. *Neuro Endocrinol Lett*. 2011;32(3):253–8.
75. Lohoff FW, Dahl JP, Ferraro TN, Arnold SE, Gallinat J, Sander T, Berrettini WH. Variations in the Vesicular Monoamine Transporter 1 Gene (VMAT1/SLC18A1) are Associated with Bipolar I Disorder. *Neuropsychopharmacology*. 2006 Dec;31(12):2739–47.
76. Avelar AJ, Juliano SA, Garris PA. Amphetamine augments vesicular dopamine release in the dorsal and ventral striatum through different mechanisms. *J Neurochem*. 2013 May;125(3):373–85.

77. Brown JM. A Single Methamphetamine Administration Rapidly Decreases Vesicular Dopamine Uptake. *J Pharmacol Exp Ther.* 2002 Aug 1;302(2):497–501.
78. Nakanishi N, Onozawa S, Matsumoto R, Hasegawa H, Yamada S. Cyclic AMP-Dependent Modulation of Vesicular Monoamine Transport in Pheochromocytoma Cells. *J Neurochem.* 1995 Nov 23;64(2):600–7.
79. Kirshner N. Uptake of Catecholamines by a Particular Fraction of the Adrenal Medulla. *J Biol Chem.* 1962 Jul;237(7):2311–7.
80. Henry JP, Sagné C, Botton D, Isambert MF, Gasnier B. Molecular Pharmacology of the Vesicular Monoamine Transporter. *Adv Pharmacol.* 1998;42:236–9.
81. German CL, Baladi MG, McFadden LM, Hanson GR, Fleckenstein AE. Regulation of the Dopamine and Vesicular Monoamine Transporters: Pharmacological Targets and Implications for Disease. *Pharmacol Rev.* 2015 Sep 25;67(4):1005–24.
82. Gilchrist A, Mazzoni MR, Dineen B, Dice A, Linden J, Proctor WR, Lupica CR, Dunwiddie TV, Hamm HE. Antagonists of the Receptor-G Protein Interface Block G_i -coupled Signal Transduction. *J Biol Chem.* 1998 Jun 12;273(24):14912–9.
83. Gilchrist A, Vanhauwe JF, Li A, Thomas TO, Voyno-Yasenetskaya T, Hamm HE. $G\alpha$ Minigenes Expressing C-terminal Peptides Serve as Specific Inhibitors of Thrombin-mediated Endothelial Activation. *J Biol Chem.* 2001 Jul 13;276(28):25672–9.
84. Eiden LE, Weihe E. VMAT2: a dynamic regulator of brain monoaminergic neuronal function interacting with drugs of abuse: VMAT2 and addiction. *Ann N Y Acad Sci.* 2011 Jan;1216(1):86–98.
85. Nakanishi N, Onozawa S, Matsumoto R, Kurihara K, Ueha T, Hasegawa H, Minami N. Effects of protein kinase inhibitors and protein phosphatase inhibitors on cyclic AMP-dependent down-regulation of vesicular monoamine transport in pheochromocytoma PC12 cells. *FEBS Lett.* 1995 Jul 24;368(3):411–4.
86. Ahnert-Hilger G. The heterotrimeric G protein Go2 regulates catecholamine uptake by secretory vesicles. *EMBO J.* 1998 Jan 15;17(2):406–13.
87. Pahner I. Subunit composition and functional properties of G-protein heterotrimers on rat chromaffin granules. *Eur J Cell Biol.* 2002 Aug;81(8):449–56.
88. Brunk I, Blex C, Rachakonda S, Höltje M, Winter S, Pahner I, Walther DJ, Ahnert-Hilger G. The First Luminal Domain of Vesicular Monoamine Transporters Mediates G-protein-dependent Regulation of Transmitter Uptake. *J Biol Chem.* 2006 Nov 3;281(44):33373–85.

89. Winter S. G o2 Regulates Vesicular Glutamate Transporter Activity by Changing Its Chloride Dependence. *J Neurosci*. 2005 May 4;25(18):4672–80.
90. Zigmond R. Acute Regulation Of Tyrosine Hydroxylase By Nerve Activity And By Neurotransmitters Via Phosphorylation. *Annu Rev Neurosci*. 1989 Jan 1;12(1):415–61.
91. Haycock JW. Four Forms of Tyrosine Hydroxylase Are Present in Human Adrenal Medulla. *J Neurochem*. 1991 Jun;56(6):2139–42.
92. Knoth J, Isaacs JM, Njus D. Amine Transport in Chromaffin Granule Ghosts. *J Biol Chem*. 1981 Jul 10;254(13):6541–6453.
93. Wimalasena DS, Wimalasena K. Kinetic Evidence for Channeling of Dopamine between Monoamine Transporter and Membranous Dopamine- β -monooxygenase in Chromaffin Granule Ghosts. *J Biol Chem*. 2004 Apr 9;279(15):15298–304.

CURRICULUM VITAE

